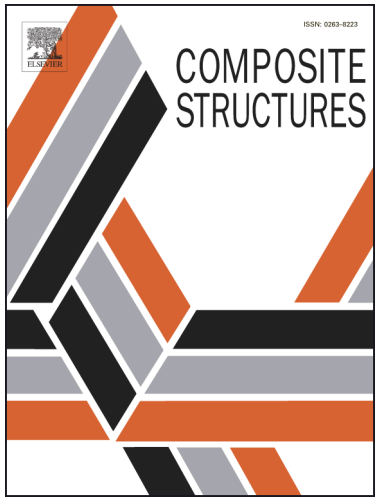

Thermoelastic Vibration and Stability of Temperature-Dependent Carbon Nanotube-Reinforced Composite Plates

Fiorenzo A. Fazzolari

PII: S0263-8223(18)30608-1
DOI: https://doi.org/10.1016/j.compstruct.2018.04.026
Reference: COST 9580

To appear in: *Composite Structures*

Received Date: 11 February 2018
Accepted Date: 3 April 2018

Please cite this article as: Fazzolari, F.A., Thermoelastic Vibration and Stability of Temperature-Dependent Carbon Nanotube-Reinforced Composite Plates, *Composite Structures* (2018), doi: https://doi.org/10.1016/j.compstruct.2018.04.026

Thermoelastic Vibration and Stability of Temperature-Dependent Carbon Nanotube-Reinforced Composite Plates

Fiorenzo A. Fazzolari[1,*]

University of Liverpool, School of Engineering, Brownlow Hill, Liverpool, L69 3GH, UK

Abstract

The present article investigates the thermoelastic vibration and stability characteristics of carbon nanotube-reinforced composite (CNTRC) plates in thermal environment. The CNTRC plates are made up of four different types of uniaxially aligned reinforcements. The single-walled carbon nanotubes (SWCNTs) reinforcement is either uniformly distributed (UD) or functionally graded (FG) according to linear functions of the thickness direction. The material properties, of both matrix and CNTs, are temperature-dependent and the effective elastic coefficients are evaluated by using a micromechanical model. The governing equations (GEs) are derived in their weak-form by using Hamilton's Principle in conjunction with the method of the power series expansion of the displacement components. The Ritz method, based on highly stable trigonometric trial functions, is used as solution technique. Convergence and stability of the proposed formulation have been thoroughly analyzed by assessing many higher-order plate models. Thermal and mechanical pre-stresses are taken into account. Moreover, the effect of significant parameters such as length-to-thickness ratio, volume fraction, aspect ratio, loading-type, CNTs distribution as well as boundary conditions is discussed.

Keywords: Quasi-3D plate theories, Thermoelastic Vibration, Elastic stability, FG-CNTRC plates, Temperature-dependent materials, Ritz method.

*Corresponding author: Tel:+44 (0)151 794 5227

Email address: Fiorenzo.Fazzolari@liverpool.ac.uk (Fiorenzo A. Fazzolari)

[1]Department of Mechanical, Materials and Aerospace Engineering

1. Introduction

Amongst a significant amount of reinforcement typologies used in the fabrication of advanced composite structures, carbon nanotubes (CNTs) have attracted a considerable interest in the recent few years. CNTs have been discovered at the beginning of the nineties by Iijima [1]. Their extraordinary mechanical, thermal and electrical properties led Harris [2] to define them the materials of the 21st century. They have low density and high stiffness and strength aspect ratios. Once the perfect bonding between the CNTs and the polymeric matrix has been guaranteed, then they can be considered as a valid alternative to classical fiber reinforced composites. The reason behind their potential application lies in the performance enhancement found out during experimental tests. In this respect, Quian et.al [3] discovered that dispersing just the 1 wt% of multiwalled carbon nanotubes (MWCNTs) homogeneously distributed within the polystyrene matrix, resulted in (36-42)% increase in the Young's modulus and in the 25% increase of the breaking stress. Some other interesting results which show evidence of a significant improvement of the mechanical characteristics can be found in Refs. [4–8]. In real life engineering applications, the CNT-reinforced composite (CNTRC) structures assumes the form of beams, plates and shells. Then, similarly to other type of reinforced composites, their modal and stability characteristics need to be thoroughly investigated. In this respect, various analysis have already been carried out. More specifically, Zhu et al. [9] analyzed the static and free vibration behaviour of CNTRC plates by using the first order shear deformation plate theory (FSDT) and the finite element method (FEM). Lei et al. [10] coped with the free vibration analysis of laminated functionally graded carbon nanotube-reinforced composite (FG-CNTRC) rectangular plates by virtue of the kp-Ritz method. The isogeometric analysis of FG-CNTRC plates via a higher-order shear deformation theory (HSDT) was performed by Phung-Van et al. [11]. Alibeigloo and Emtehani [12] dealt with static and free vibration analyses FG-CNTRC plates by means of the generalized differential quadrature (GDQ) method. The same author [13] provided a three dimensional solution based on the theory of elasticity for FG-CNTRC plates embedded in piezoelectric layers. Arani et al. [14] studied the elastic stability of laminated composite rectangular plates reinforced by single-walled carbon nanotubes (SWCNTs) by using both analytical and finite element methods. Malekzadeh and Shojaee [15] analysed the buckling characteristics of quadrilateral laminated plates with CNTs-reinforced layers. Ray and Batra [16] derived the effective properties of CNTs and piezoelectric fibre reinforced hybrid smart composites. The

same authors [17] analyzed the behaviour of a SWCNT-reinforced piezoelectric composite for active control of smart structures. Zhang and Liew [18] provided a vibration analysis of FG-CNTRC thick plates resting on elastic foundations by using the element free IMLS-Ritz method. Thai et al. [19] have recently developed a naturally stabilized integration meshfree formulation for the analysis of CNTRC plates. Results were provided in terms of dimensionless stresses, displacements and natural frequencies. Bending and free vibration response of FG graphene (GP) and CNTRC composite plates have been compared by Marcias et al. [20]. The results showed the superiority of the GPRC plates in terms of load bearing capacity for both fully aligned and randomly oriented graphene sheets. The low velocity impact modeling of FG-CNTRC plates with arbitrary geometry and general boundary conditions has been studied by Fallah et al. [21]. Aeroelastic characteristics of FG-CNTRC plates under a supersonic flow were investigated by Fazelzadeh at al. [22]. Ansari et al. [23] coped with the free vibration analysis of FG-CNTRC elliptical plates by using the moving last square (MLS) meshless method. The nonlinear free vibration analysis of FG-CNTRC quadrilateral plates have been investigate by Setoodeh and Shojaee [24]. The authors used the GDQ method in conjunction with the transformed weighing coefficients (TW-DQ), specifically introduced to solve geometrically nonlinear free vibration problems. Kumar and Srinivas [25] investigated the free vibration, buckling and bending behavior of FG-MWCNTs reinforced polymer composite plates using the layer-wise formulation. A comprehensive free vibration analysis of SWCNTs with elastic boundary conditions have been proposed by Jiang et al. [26]. Semi-analytical solutions to buckling and free vibration analysis of CNTRC thin plates were proposed by Wang et al. [27].

In this respect, it is also interesting to note that the use of exact solution techniques for both free vibration and buckling analyses, such as those proposed in Refs. [28–31], could be, in a relatively easy manner, extended to the analysis of FG-CNTRC plates.

As regard the use of CNTs-reinforced composite structures related to thermal applications, it is worth mentioning the following articles. Zhang and Shen [32] predicted the temperature-dependent elastic properties of SWCNTs by using molecular dynamics (MD) simulation. The same authors [33] always by means of MD simulation carried out buckling and postbuckling analysis of SWCNTs in thermal environments. Subsequently in Ref. [34], they extended the thermal buckling and postbuckling analysis to FG-CNTRC plates. Recently, Shen and Wang [35] dealt with the nonlinear vibration of compressed and thermally postbuckled CNTRC

plates resting on elastic foundations. The same author [36] investigated also the nonlinear vibration of CNTRC plates in thermal environments. Shen et. al [37] studied also the vibration of thermally postbuckled sandwich plates with CNTRC face sheets resting on elastic foundations. Alibeigloo and Liew [38] carried out a thermoelastic analysis of FG-CNTRC plates using the theory of elasticity.

In the present article the method of power series expansion of displacement components, extensively employed in the analysis of laminated composite and FGM beams, plates and shells [39–47] has been extended to provide a comprehensive thermoelastic vibration and elastic stability analysis of CNTRC plates. In particular, the advanced quasi-3D plate theories with hierarchical capabilities have been developed and then validated and assessed against results available in literature. Highly stable trigonometric Ritz functions have been used in the approximation. A thorough convergence analysis has also been carried out. Both modal and stability characteristics of the CNTRC plates under investigation have been studied while varying significant parameters such as the environmental temperature, length-to-thickness ratio, volume fraction, aspect ratio, CNTs distribution as well as boundary conditions. Finally, from all of the carried out numerical analyses some conclusions have been drawn.

2. Effective material properties of CNTRC plates and temperature dependency

The present analysis takes into account four different types of CNTRC plates as shown in Fig. 1. More specifically, the mathematical laws which characterise these distributions are given as follows

$$V_{CNT} = V^*_{CNT} \qquad \text{UD} \quad \text{CNTRC} \tag{1}$$

$$V_{CNT}(z) = \left(1 + \frac{2\,z}{h}\right) V^*_{CNT} \qquad \text{FG-V} \quad \text{CNTRC} \tag{2}$$

$$V_{CNT}(z) = 2\left(1 - \frac{2\,|z|}{h}\right) V^*_{CNT} \qquad \text{FG-O} \quad \text{CNTRC} \tag{3}$$

$$V_{CNT}(z) = 2\left(\frac{2\,|z|}{h}\right) V^*_{CNT} \qquad \text{FG-X} \quad \text{CNTRC} \tag{4}$$

where

$$V^*_{CNT} = \frac{w_{CNT}}{w_{CNT} + \frac{\rho_{CNT}}{\rho_m} - \frac{\rho_{CNT}}{\rho_m} w_{CNT}} \tag{5}$$

is the CNTs volume fraction, w_{CNT} is the mass fraction of the carbon nanotube in the composite plate; ρ_m and ρ_{CNT} are the densities of the matrix and carbon nanotube, respectively. It should be noted that the overall mass fraction w_{CNT} of the carbon nanotubes remains

the same for all the CNTRC plates considered. The quantities V_{CNT} and V_m represent the volume fraction of the CNTs and the polymeric matrix, respectively, and they are related by the equation $V_{CNT}(z) + V_m(z) = 1$. The effective material properties of the two-phase nanocomposite, based on the mixture of the CNTs and an isotropic polymer can be derived by using either the Elshelby-Mori-Tanaka micromechanical model [48–50] or the extended Voigt's rule of mixture (ROM) [51]. In the present article the latter has been adopted and the effective material properties can be expressed accordingly as follows

$$\begin{aligned}
E_{11}(z,T) &= \eta_1 V_{CNT}(z)\, E_{11}^{CNT}(T) + V_m(z)\, E^m(T);\\
\frac{\eta_2}{E_{22}(z,T)} &= \frac{V_{CNT}(z)}{E_{22}^{CNT}(T)} + \frac{V_m(z)}{E_{22}^m(T)};\\
\frac{\eta_3}{G_{12}(z,T)} &= \frac{V_{CNT}(z)}{G_{12}^{CNT}(T)} + \frac{V_m(z)}{G_{12}^m(T)};\\
\nu_{12}(z) &= V_{CNT}(z)\, \nu_{12}^{CNT} + V_m(z)\, \nu_{12}^m;\\
\rho(z) &= V_{CNT}(z)\, \rho_{CNT} + V_m(z)\, \rho_m;
\end{aligned} \tag{6}$$

where E_{11}^{CNT}, E_{22}^{CNT}, G_{12}^{CNT}, ν_{12}^{CNT} and ρ_{CNT} are the Young's modulii, the shear modulus, the Poisson's ratio and the density of the SWCNTs, respectively; E_m, G_m, ν_{12}^m and ρ_m represent the corresponding material properties of the isotropic matrix. In order to take into account the scale-dependency of the effective material properties of the CNTs, the efficiency parameters η_i with $i = 1, 2, 3$ have been introduced. The latter have been computed by comparing the results obtained via Molecular Dynamic (MD) simulations with those evaluated from the ROM. The thermal expansion coefficients in the longitudinal and transverse direction, respectively, are given as follows

$$\begin{aligned}
\alpha_{11}(z,T) &= \frac{V_{CNT}(z)\, E_{11}^{CNT}(T)\, \alpha_{11}^{CNT}(T) + V_m(z)\, E_m(T)\, \alpha^m(T)}{V_{CNT}(z)\, \alpha_{11}^{CNT}(T) + V_m(z)\, \alpha^m(T)};\\
\alpha_{22}(z,T) &= \left(1+\nu_{12}^{CNT}\right) V_{CNT}(z)\, \alpha_{22}^{CNT} + \left(1+\nu_{12}^m\right) V_m(z)\, \alpha_m(T) - \nu_{12}(z)\, \alpha_{11}^{CNT}(T)
\end{aligned} \tag{7}$$

where α_{11}^{CNT}, α_{22}^{CNT} and α^m are the thermal expansion coefficients of the CNT and the matrix. It should be borne in mind that in the present article the materials are considered temperature-dependent. Thus, the Young's moduli, the shear modulus and the thermal expansion coefficients, of both matrix and CNTs, are function of temperature T and the plate-thickness coordinate z. In particular, in the present investigation the matrix is made up of Poly Methyl Methacrylate (PMMA) whose material properties have a temperature

dependency according to the following equations:

$$E_m(T) = (3.52 - 0.0034\,T)\ GPa;\ \ \alpha_m(T) = 45\,(1 + 0.0005\,\Delta T) \times \frac{10^{-6}}{K};\ \ \rho_m = 1150\,\frac{Kg}{m^3};$$
$$\nu_m = 0.34 \tag{8}$$

The CNTs chosen as reinforcement are the armchair (10,10) SWCNTs, whose material properties at room temperature $T_0 = 300\,K$ are reported in Fig. 1, whilst their temperature dependency is given as follows [35]

$$E_{11}^{CNT}(T) = \left(6.18387 - 0.00286\ T + 4.22867 \times 10^6\ T^2 - 2.2724 \times 10^9\ T^3\right) TPa;$$
$$E_{22}^{CNT}(T) = \left(7.75348 - 0.00358\ T + 5.30057 \times 10^6\ T^2 - 2.84868 \times 10^9\ T^3\right) TPa;$$
$$G_{12}^{CNT}(T) = \left(1.80126 + 7.7845 \times 10^4\ T - 1.1279 \times 10^6\ T^2 + 4.93484 \times 10^{10}\ T^3\right) TPa;$$
$$\alpha_{11}^{CNT}(T) = \left(-1.12148 + 0.02289\ T - 2.88155 \times 10^5\ T^2 + 1.13253 \times 10^8\ T^3\right) \frac{10^{-6}}{K};$$
$$\alpha_{22}^{CNT}(T) = \left(5.43874 - 9.95498 \times 10^4\ T + 3.13525 \times 10^7\ T^2 - 3.56332 \times 10^{12}\ T^3\right) \frac{10^{-6}}{K};$$
$$\nu_{12}^{CNT} = 0.175; \quad \rho^{CNT} = 1400\,\frac{Kg}{m^3} \tag{9}$$

Where $T = T_0 + \Delta T$. The variation of the CNTs thermo-mechanical properties with the temperature as shown in Eq. (9) are reliable in the temperature range $300\,K \leq T \leq 1000\,K$. Table 1 shows the temperature-dependent material properties for an armchair $(10, 10)$ SWCNT evaluated by means of MD simulation. Table 2 provides the comparison of the Young's modulii E_{11} and E_{22} computed by virtue of MD [52] and those evaluated by using the rule of mixture (ROM). An excellent agreement can be observed.

3. Geometric and constitutive relations

The nomenclature and geometry of the CNTRC plate are shown in Fig. 1. In addition to that, it is useful to recall that, the reference plane, often referred to as plate middle-surface, which lies in the plane (xy) is named Ω whilst the z coordinate is referred to as thickness coordinate. According to the classical nomenclature used in literature, the length of the plate in the x and y-direction is indicated by a and b, respectively, while the thickness dimension is denoted as h. Consistently to the reference coordinate system the stress and strain vectors are indicated as follows

$$\boldsymbol{\sigma} = \left\{ \begin{array}{cccccc} \sigma_{xx} & \sigma_{yy} & \tau_{xy} & \tau_{xz} & \tau_{yz} & \sigma_{zz} \end{array} \right\}^T, \quad \boldsymbol{\varepsilon} = \left\{ \begin{array}{cccccc} \varepsilon_{xx} & \varepsilon_{yy} & \gamma_{xy} & \gamma_{xz} & \gamma_{yz} & \varepsilon_{zz} \end{array} \right\}^T \tag{10}$$

The strain-displacement relations are

$$\boldsymbol{\varepsilon} = \mathbf{D}\mathbf{u} \tag{11}$$

where $\mathbf{D}$ and $\mathbf{u}$ are a differential matrix operator and the displacement vector, defined as follows

$$\mathbf{D} = \begin{bmatrix} \frac{\partial}{\partial x} & 0 & 0 \\ 0 & \frac{\partial}{\partial y} & 0 \\ \frac{\partial}{\partial y} & \frac{\partial}{\partial x} & 0 \\ \frac{\partial}{\partial z} & 0 & \frac{\partial}{\partial x} \\ 0 & \frac{\partial}{\partial z} & \frac{\partial}{\partial y} \\ 0 & 0 & \frac{\partial}{\partial z} \end{bmatrix}, \quad \mathbf{u} = \begin{Bmatrix} u_x \\ u_y \\ u_z \end{Bmatrix} \tag{12}$$

The 3D constitutive equations related to thermoelastic problem can be written in the following compact form,

$$\boldsymbol{\sigma} = \mathbf{C}(z,T)\,\boldsymbol{\varepsilon} - \boldsymbol{\Xi}(z,T)\,\Delta T \tag{13}$$

where ΔT is the temperature variation and $\boldsymbol{\Xi}$ is the thermoelastic coupling coefficient which is given as

$$\boldsymbol{\Xi}(z,T) = \mathbf{C}(z,T)\,\boldsymbol{\alpha}(z,T) \tag{14}$$

$\boldsymbol{\alpha}$ is the vector including the coefficients of thermal expansion and assumes the following form

$$\boldsymbol{\alpha}(z,T) = \left\{ \begin{array}{ccccccc} \alpha_{11}(z,T) & \alpha_{22}(z,T) & 0 & 0 & 0 & \alpha_{33}(z,T) \end{array} \right\}^T \tag{15}$$

and $\mathbf{C}$ is the constitutive matrix,

$$\mathbf{C}(z,T) = \begin{bmatrix} C_{11}(z,T) & C_{12}(z,T) & 0 & 0 & 0 & C_{13}(z,T) \\ C_{12}(z,T) & C_{22}(z,T) & 0 & 0 & 0 & C_{23}(z,T) \\ 0 & 0 & C_{66}(z,T) & 0 & 0 & 0 \\ 0 & 0 & 0 & C_{44}(z,T) & 0 & 0 \\ 0 & 0 & 0 & 0 & C_{55}(z,T) & 0 \\ C_{31}(,T) & C_{32}(z,T) & 0 & 0 & 0 & C_{33}(z,T) \end{bmatrix} \tag{16}$$

where the explicit expression of $\alpha_{ii}(z,T)$ and $C_{ij}(z,T)$ in terms of Young's modulii and Poisson's ratios can be found in standard composite materials textbook [53, 54] and represent the effective elastic coefficients. In this respect, it is also useful to note that the effective Young's modulii, Poisson's ratios and shear modulus are evaluated via an accurate micromechanical model (see Eq. (1) for further details).

4. Hierarchical plate models

Since the first pioneering derivation of the classical structural models, based on the Newtonian Mechanics (NM), such as those proposed by Kircchoff [55] and Reissner-Mindlin [56, 57], scientists and researchers have focused their attention and efforts on the development of increasingly accurate structural theories. By relying on the Lagrangian Mechanics (LM), the method of power series expansion of the displacement components represents a generalisation of the aforementioned classical theories. In essence, each displacement component in the displacement field is expanded at any desired order according to the computational cost and the level of accuracy required. The methodology can be traced back to Washitsu [58] and more recently Matsunaga [59] and Carrera [60, 61]. However, only in the last three decades these new approach to the theory of structures has been fully exploited. This has only been possible due to the significant enhancement in the computer performances. In this respect, the advanced structural models have been successfully implemented in computer programs and used both for real life engineering applications and for fundamental research.
According to this, relatively new, approach the most general displacement field assumes the following form

$$\begin{aligned} u_x(x,y,z,t) &= \sum_{\tau_{u_x}=1}^{N_{u_x}} F_{\tau_{u_x}}(z)\; u_{x_{\tau_{u_x}}}(x,y,t) \\ u_y(x,y,z,t) &= \sum_{\tau_{u_y}=1}^{N_{u_y}} F_{\tau_{u_y}}(z)\; u_{y_{\tau_{u_y}}}(x,y,t) \\ u_z(x,y,z,t) &= \sum_{\tau_{u_z}=1}^{N_{u_z}} F_{\tau_{u_z}}(z)\; u_{z_{\tau_{u_z}}}(x,y,t) \end{aligned} \tag{17}$$

where $F_{\tau_{u_x}}$, $F_{\tau_{u_y}}$, $F_{\tau_{u_z}}$ are the thickness functions. They can be generic functions of the plate-thickness coordinate. Their purpose is to accurately describe the plate kinematics through-the-thickness direction. To this aim, in the present investigation Taylor polynomials have been chosen. The functions $u_{x\tau_{u_x}}$, $u_{y\tau_{u_y}}$, $u_{z\tau_{u_z}}$ represent the displacement vector components and, finally, N_{u_x}, N_{u_y} and N_{u_z} are the orders of expansion of the in-plane and out-of-plane displacement components, respectively.

5. Theoretical Formulation

In the derivation of what follows Hamilton's principle (HP) is employed to derive the governing equations in their weak form. The solution is then sought by using the Hierarchical

Trigonometric Ritz Formulation (HTRF). In its classical from HP can be written as

$$\int_{t_1}^{t^2} \delta\mathcal{L}\,\mathrm{d}t = 0 \tag{18}$$

where t_1 and t_2 are the initial and the generic instant of time; $\mathcal{L}$ is the Lagrangian which assumes the following form

$$\mathcal{L} = T - \Pi \quad \text{where} \quad \Pi = \Phi_e + \Phi_\sigma \tag{19}$$

T is the kinetic energy and Π is the total potential energy of the system; Φ_e and Φ_σ are the potential strain energy and the potential energy due to the thermal and/or mechanical initial stresses, respectively. HP can be alternatively written in terms of displacements as follows

$$\begin{aligned}
\int_{t_1}^{t^2} \Bigg\{ \int_V \Big[& C_{11}(z,T)\,\delta u_{x,x}\,u_{x,x} + C_{66}(z,T)\,\delta u_{x,y}\,u_{x,y} + C_{55}(z,T)\,\delta u_{x,z}\,u_{x,z} + \\
& C_{12}(z,T)\,\delta u_{x,x}\,u_{y,y} + C_{66}(z,T)\,\delta u_{x,y}\,u_{y,x} + \\
& C_{13}(z,T)\,\delta u_{x,x}\,u_{z,z} + C_{55}(z,T)\,\delta u_{x,z}\,u_{z,x} + \\
& C_{12}(z,T)\,\delta u_{y,x}\,u_{x,y} + C_{66}(z,T)\,\delta u_{y,y}\,u_{x,x} + \\
& C_{22}(z,T)\,\delta u_{y,y}\,u_{y,y} + C_{66}(z,T)\,\delta u_{y,x}\,u_{y,x} + C_{44}(z,T)\,\delta u_{y,z}\,u_{y,z} + \\
& C_{44}(z,T)\,\delta u_{y,y}\,u_{z,z} + C_{23}(z,T)\,\delta u_{y,z}\,u_{z,y} + \\
& C_{13}(z,T)\,\delta u_{z,x}\,u_{x,z} + C_{55}(z,T)\,\delta u_{z,z}\,u_{x,x} + \\
& C_{44}(z,T)\,\delta u_{z,y}\,u_{y,z} + C_{23}(z,T)\,\delta u_{z,z}\,u_{y,y} + \\
& C_{44}(z,T)\,\delta u_{z,z}\,u_{z,z} + C_{55}(z,T)\,\delta u_{z,x}\,u_{z,x} + C_{33}(z,T)\,\delta u_{z,y}\,u_{z,y} \Big]\mathrm{d}V + \\
\int_V \Big[& \tilde{\sigma}_{xx}^{(0)}\,\delta u_{x,x}\,u_{x,x} + \tilde{\sigma}_{yy}^{(0)}\,\delta u_{x,y}\,u_{x,y} + \tilde{\tau}_{xy}^{(0)}\,\delta u_{x,x}\,u_{x,y} \\
& \tilde{\sigma}_{xx}^{(0)}\,\delta u_{y,x}\,u_{y,x} + \tilde{\sigma}_{yy}^{(0)}\,\delta u_{y,y}\,u_{y,y} + \tilde{\tau}_{xy}^{(0)}\,\delta u_{y,x}\,u_{y,y} \\
& \tilde{\sigma}_{xx}^{(0)}\,\delta u_{z,x}\,u_{z,x} + \tilde{\sigma}_{yy}^{(0)}\,\delta u_{z,y}\,u_{z,y} + \tilde{\tau}_{xy}^{(0)}\,\delta u_{z,x}\,u_{z,y} \Big]\mathrm{d}V + \\
\int_V \Big[& \rho\left(\delta\dot{u}_x\,\dot{u}_x + \delta\dot{u}_y\,\dot{u}_y + \delta\dot{u}_z\,\dot{u}_z\right) \Big]\mathrm{d}V \Bigg\}\mathrm{d}t = 0
\end{aligned} \tag{20}$$

where ρ is the material density; $\tilde{\sigma}_{xx}^{(0)}$, $\tilde{\sigma}_{yy}^{(0)}$ and $\tilde{\tau}_{xx}^{(0)}$ are the initial stress due to mechanical, thermal or thermo-mechanical effects. The $,x$; $,y$; and $,z$ represent derivative with respect to these variables, and $\dot{()}$ indicates the time derivative. It should also be noted that in Eq. (20), it has been highlighted the dependency of the effective elastic coefficients from both the thickness coordinate z and the temperature T. The former is due to the FG-CNTs distributions the latter is related to the temperature-dependency of both matrix and CNTs (see Eqs. (8) and (9) for more information).

5.1. The Hierarchical Ritz Formulation

In the Ritz method the displacement amplitude vector components $u_{x_{\tau_{u_x}}}$, $u_{y_{\tau_{u_y}}}$ and $u_{z_{\tau_{u_z}}}$ are expressed in series expansion and the displacement field assumes the following form

$$\begin{aligned} u_x(x,y,z,t) &= \sum_{i=1}^{\mathcal{N}} \sum_{\tau_{ux}=1}^{N_{u_x}} U_{x\tau_{u_x}i}(t)\, F_{\tau_{u_x}}(z)\, \psi_{x_i}(x,y)\, \mathrm{e}^{\mathrm{i}\omega t} \\ u_y(x,y,z,t) &= \sum_{i=1}^{\mathcal{N}} \sum_{\tau_{uy}=1}^{N_{u_y}} U_{y\tau_{u_y}i}(t)\, F_{\tau_{u_y}}(z)\, \psi_{y_i}(x,y)\, \mathrm{e}^{\mathrm{i}\omega t} \\ u_z(x,y,z,t) &= \sum_{i=1}^{\mathcal{N}} \sum_{\tau_{u_z}=1}^{N_{u_z}} U_{z\tau_{u_z}i}(t)\, F_{\tau_{u_z}}(z)\, \psi_{z_i}(x,y)\, \mathrm{e}^{\mathrm{i}\omega t} \end{aligned} \tag{21}$$

where $\mathcal{N}$ indicates the order of expansion in the Ritz approximation; $U_{x\tau_{u_x}i}$, $U_{y\tau_{u_y}i}$, $U_{z\tau_{u_z}i}$ are the time-dependent unknown coefficients; and ψ_{x_i}, ψ_{y_i}, ψ_{z_i} are the Ritz functions appropriately selected with respect to the features of the problem under investigation. Convergence to the exact solution is guaranteed if the Ritz functions are admissible functions in the used variational principle (more information can be found in Refs. [39, 40, 62, 63]).

5.2. Explicit form of the virtual potential and kinetic energy

Once Eq.(21) is substitute into Eq.(20), it is then possible to express all of the energy contributions appearing in Hamilton's principle, namely $\delta\Phi_e$, $\delta\Phi_\sigma$ and δT, in terms of Ritz functions, effective elastic coefficients and thickness functions. The integral subscripts represent the in-plane and out-of-plane integration domains, and are indicated as follows

$$\mathcal{A}_x \in [0,a]\,; \quad \mathcal{A}_y \in [0,b]\,; \quad \mathcal{A}_z \in [-h/2, h/2] \tag{22}$$

5.2.1. Virtual potential strain energy

The $\delta\Phi_e$ can actually be considered as the summation of the following nine contributions

$$\begin{aligned} \delta\Phi_e^{u_x u_x} = \delta U_{x\tau_{u_x}i}(t) \Big[& \int_{\mathcal{A}_z} C_{11}(z,T)\, F_{\tau_{u_x}}(z)\, F_{s_{u_x}}(z)\,\mathrm{d}z \int_{\mathcal{A}_x}\int_{\mathcal{A}_y} \psi_{x_{u_x i},x}(x,y)\, \psi_{x_{u_x j},x}(x,y)\,\mathrm{d}x\,\mathrm{d}y \\ & + \int_{\mathcal{A}_z} C_{66}(z,T)\, F_{\tau_{u_x}}(z)\, F_{s_{u_x}}(z)\,\mathrm{d}z \int_{\mathcal{A}_x}\int_{\mathcal{A}_y} \psi_{x_{u_x i},y}(x,y)\, \psi_{x_{u_x j},y}(x,y)\,\mathrm{d}x\,\mathrm{d}y \\ & + \int_{\mathcal{A}_z} C_{55}(z,T)\, F_{\tau_{u_x},z}(z)\, F_{s_{u_x},z}(z)\,\mathrm{d}z \int_{\mathcal{A}_x}\int_{\mathcal{A}_y} \psi_{x_{u_x i}}(x,y)\, \psi_{x_{u_x j}}(x,y)\,\mathrm{d}x\,\mathrm{d}y \Big] U_{xs_{u_x}j}(t) \end{aligned}$$

$$\begin{aligned} \delta\Phi_e^{u_x u_y} = \delta U_{x\tau_{u_x}i}(t) \Big[& \int_{\mathcal{A}_z} C_{12}(z,T)\, F_{\tau_{u_x},x}(z)\, F_{s_{u_y},y}(z)\,\mathrm{d}z \int_{\mathcal{A}_x}\int_{\mathcal{A}_y} \psi_{x_{u_x i}}(x,y)\, \psi_{y_{u_y j}}(x,y)\,\mathrm{d}x\,\mathrm{d}y \\ & + \int_{\mathcal{A}_z} C_{66}(z,T)\, F_{\tau_{u_x}}(z)\, F_{s_{u_y}}(z)\,\mathrm{d}z \int_{\mathcal{A}_x}\int_{\mathcal{A}_y} \psi_{x_{u_x i},y}(x,y)\, \psi_{y_{u_y j},x}(x,y)\,\mathrm{d}x\,\mathrm{d}y \Big] U_{ys_{u_y}j}(t) \end{aligned}$$

$$\delta\Phi_e^{u_x u_z} = \delta U_{x\tau_{u_x} i}(t)\Big[\int_{\mathcal{A}_z} C_{13}(z,T)\, F_{\tau_{u_x}}(z)\, F_{s_{u_z},z}(z)\,\mathrm{d}z \int_{\mathcal{A}_x}\int_{\mathcal{A}_y} \psi_{x_{u_x i},x}(x,y)\,\psi_{z_{u_z j}}(x,y)\,\mathrm{d}x\,\mathrm{d}y + \int_{\mathcal{A}_z} C_{55}(z,T)\, F_{\tau_{u_x},z}(z)\, F_{s_{u_z}}(z)\,\mathrm{d}z \int_{\mathcal{A}_x}\int_{\mathcal{A}_y} \psi_{x_{u_x i}}(x,y)\,\psi_{z_{u_z j},x}(x,y)\,\mathrm{d}x\,\mathrm{d}y\Big] U_{zs_{u_z}j}(t)$$

$$\delta\Phi_e^{u_y u_x} = \delta U_{y\tau_{u_y} i}(t)\Big[\int_{\mathcal{A}_z} C_{12}(z,T)\, F_{\tau_{u_y}}(z)\, F_{s_{u_x}}(z)\,\mathrm{d}z \int_{\mathcal{A}_x}\int_{\mathcal{A}_y} \psi_{y_{u_y i},y}(x,y)\,\psi_{x_{u_x j},x}(x,y)\,\mathrm{d}x\,\mathrm{d}y + \int_{\mathcal{A}_z} C_{66}(z,T)\, F_{\tau_{u_y}}(z)\, F_{s_{u_x}}(z)\,\mathrm{d}z \int_{\mathcal{A}_x}\int_{\mathcal{A}_y} \psi_{y_{u_y i},x}(x,y)\,\psi_{x_{u_x j},y}(x,y)\,\mathrm{d}x\,\mathrm{d}y\Big] U_{xs_{u_x}j}(t)$$

$$\delta\Phi_e^{u_y u_y} = \delta U_{y\tau_{u_y} i}(t)\Big[\int_{\mathcal{A}_z} C_{22}(z,T)\, F_{\tau_{u_y}}(z)\, F_{s_{u_y}}(z)\,\mathrm{d}z \int_{\mathcal{A}_x}\int_{\mathcal{A}_y} \psi_{y_{u_y i},y}(x,y)\,\psi_{y_{u_y j},y}(x,y)\,\mathrm{d}x\,\mathrm{d}y + \int_{\mathcal{A}_z} C_{66}(z,T)\, F_{\tau_{u_y}}(z)\, F_{s_{u_y}}(z)\,\mathrm{d}z \int_{\mathcal{A}_x}\int_{\mathcal{A}_y} \psi_{y_{u_y i},y}(x,y)\,\psi_{y_{u_y j},x}(x,y)\,\mathrm{d}x\,\mathrm{d}y + \int_{\mathcal{A}_z} C_{44}(z,T)\, F_{\tau_{u_y},z}(z)\, F_{s_{u_y},z}(z)\,\mathrm{d}z \int_{\mathcal{A}_x}\int_{\mathcal{A}_y} \psi_{y_{u_y i}}(x,y)\,\psi_{y_{u_y j}}(x,y)\,\mathrm{d}x\,\mathrm{d}y\Big] U_{ys_{u_y}j}(t)$$

$$\delta\Phi_e^{u_y u_z} = \delta U_{y\tau_{u_y} i}(t)\Big[\int_{\mathcal{A}_z} C_{44}(z,T)\, F_{\tau_{u_y},z}(z)\, F_{s_{u_z}}(z)\,\mathrm{d}z \int_{\mathcal{A}_x}\int_{\mathcal{A}_y} \psi_{y_{u_y i}}(x,y)\,\psi_{z_{u_z j},y}(x,y)\,\mathrm{d}x\,\mathrm{d}y + \int_{\mathcal{A}_z} C_{23}(z,T)\, F_{\tau_{u_y}}(z)\, F_{s_{u_z},z}(z)\,\mathrm{d}z \int_{\mathcal{A}_x}\int_{\mathcal{A}_y} \psi_{y_{u_y i},y}(x,y)\,\psi_{z_{u_z j}}(x,y)\,\mathrm{d}x\,\mathrm{d}y\Big] U_{zs_{u_z}j}(t)$$

$$\delta\Phi_e^{u_z u_x} = \delta U_{z\tau_{u_z} i}(t)\Big[\int_{\mathcal{A}_z} C_{13}(z,T)\, F_{\tau_{u_z},z}(z)\, F_{s_{u_x}}(z)\,\mathrm{d}z \int_{\mathcal{A}_x}\int_{\mathcal{A}_y} \psi_{z_{u_z i},x}(x,y)\,\psi_{x_{u_x j}}(x,y)\,\mathrm{d}x\,\mathrm{d}y + \int_{\mathcal{A}_z} C_{55}(z,T)\, F_{\tau_{u_z}}(z)\, F_{s_{u_x},z}(z)\,\mathrm{d}z \int_{\mathcal{A}_x}\int_{\mathcal{A}_y} \psi_{z_{u_z i},x}(x,y)\,\psi_{x_{u_x j}}(x,y)\,\mathrm{d}x\,\mathrm{d}y\Big] U_{xs_{u_x}j}(t)$$

$$\delta\Phi_e^{u_z u_y} = \delta U_{z\tau_{u_z} i}(t)\Big[\int_{\mathcal{A}_z} C_{44}(z,T)\, F_{\tau_{u_z}}(z)\, F_{s_{u_y},z}(z)\,\mathrm{d}z \int_{\mathcal{A}_x}\int_{\mathcal{A}_y} \psi_{z_{u_z i},y}(x,y)\,\psi_{y_{u_y j}}(x,y)\,\mathrm{d}x\,\mathrm{d}y + \int_{\mathcal{A}_z} C_{23}(z,T)\, F_{\tau_{u_z},z}(z)\, F_{s_{u_y}}(z)\,\mathrm{d}z \int_{\mathcal{A}_x}\int_{\mathcal{A}_y} \psi_{z_{u_z i}}(x,y)\,\psi_{y_{u_y j},y}(x,y)\,\mathrm{d}x\,\mathrm{d}y\Big] U_{ys_{u_y}j}(t)$$

$$\delta\Phi_e^{u_z u_z} = \delta U_{z\tau_{u_z} i}(t)\Big[\int_{\mathcal{A}_z} C_{44}(z,T)\, F_{\tau_{u_z}}(z)\, F_{s_{u_z}}(z)\,\mathrm{d}z \int_{\mathcal{A}_x}\int_{\mathcal{A}_y} \psi_{z_{u_z i},y}(x,y)\,\psi_{z_{u_z j},y}(x,y)\,\mathrm{d}x\,\mathrm{d}y + \int_{\mathcal{A}_z} C_{55}(z,T)\, F_{\tau_{u_z}}(z)\, F_{s_{u_z}}(z)\,\mathrm{d}z \int_{\mathcal{A}_x}\int_{\mathcal{A}_y} \psi_{z_{u_z i},x}(x,y)\,\psi_{z_{u_z j},x}(x,y)\,\mathrm{d}x\,\mathrm{d}y + \int_{\mathcal{A}_z} C_{33}(z,T)\, F_{\tau_{u_z},z}(z)\, F_{s_{u_z},z}(z)\,\mathrm{d}z \int_{\mathcal{A}_x}\int_{\mathcal{A}_y} \psi_{z_{u_z i}}(x,y)\,\psi_{z_{u_z j}}(x,y)\,\mathrm{d}x\,\mathrm{d}y\Big] U_{zs_{u_z}j}(t) \tag{23}$$

5.2.2. Virtual potential energy due to the initial stresses

A similar consideration can be drawn for the $\delta\Phi_\sigma$, whose contributions are given by

$$\begin{aligned}
\delta\Phi_\sigma^{u_x u_x} &= \delta_{vK}\,\delta U_{x\tau_{u_x} i}\,(t)\Big[\int_{\mathcal{A}_z}\tilde{\sigma}_{xx}F_{\tau_{u_x}}\,(z)\,F_{s_{u_x}}\,(z)\,\mathrm{d}z\int_{\mathcal{A}_x}\int_{\mathcal{A}_y}\psi_{x_{u_x}\,i,x}\,(x,y)\,\psi_{x_{u_x}\,j,x}\,(x,y)\,\mathrm{d}x\,\mathrm{d}y\\
&+\int_{\mathcal{A}_z}\tilde{\sigma}_{yy}F_{\tau_{u_x}}\,(z)\,F_{s_{u_x}}\,(z)\,\mathrm{d}z\int_{\mathcal{A}_x}\int_{\mathcal{A}_y}\psi_{x_{u_x}\,i,y}\,(x,y)\,\psi_{x_{u_x}\,j,y}\,(x,y)\,\mathrm{d}x\,\mathrm{d}y\\
&+\int_{\mathcal{A}_z}\tilde{\tau}_{xy}F_{\tau_{u_x}}\,(z)\,F_{s_{u_x}}\,(z)\,\mathrm{d}z\int_{\mathcal{A}_x}\int_{\mathcal{A}_y}\psi_{x_{u_x}\,i,x}\,(x,y)\,\psi_{x_{u_x}\,j,y}\,(x,y)\,\mathrm{d}x\,\mathrm{d}y\Big]U_{x\tau_{u_x}j}\,(t)
\end{aligned}$$

$$\begin{aligned}
\delta\Phi_\sigma^{u_y u_y} &= \delta_{vK}\,\delta U_{y\tau_{u_y} i}\,(t)\Big[\int_{\mathcal{A}_z}\tilde{\sigma}_{xx}F_{\tau_{u_y}}\,(z)\,F_{s_{u_y}}\,(z)\,\mathrm{d}z\int_{\mathcal{A}_x}\int_{\mathcal{A}_y}\psi_{y_{u_y}\,i,x}\,(x,y)\,\psi_{y_{u_y}\,j,x}\,(x,y)\,\mathrm{d}x\,\mathrm{d}y\\
&+\int_{\mathcal{A}_z}\tilde{\sigma}_{yy}F_{\tau_{u_y}}\,(z)\,F_{s_{u_y}}\,(z)\,\mathrm{d}z\int_{\mathcal{A}_x}\int_{\mathcal{A}_y}\psi_{y_{u_y}\,i,y}\,(x,y)\,\psi_{y_{u_y}\,j,y}\,(x,y)\,\mathrm{d}x\,\mathrm{d}y\\
&+\int_{\mathcal{A}_z}\tilde{\tau}_{xy}F_{\tau_{u_y}}\,(z)\,F_{s_{u_y}}\,(z)\,\mathrm{d}z\int_{\mathcal{A}_x}\int_{\mathcal{A}_y}\psi_{y_{u_y}\,i,x}\,(x,y)\,\psi_{y_{u_y}\,j,y}\,(x,y)\,\mathrm{d}x\,\mathrm{d}y\Big]U_{y\tau_{u_y}j}\,(t)
\end{aligned}$$

$$\begin{aligned}
\delta\Phi_\sigma^{u_z u_z} &= \delta U_{z\tau_{u_z} i}\,(t)\Big[\int_{\mathcal{A}_z}\tilde{\sigma}_{xx}F_{\tau_{u_z}}\,(z)\,F_{s_{u_z}}\,(z)\,\mathrm{d}z\int_{\mathcal{A}_x}\int_{\mathcal{A}_y}\psi_{z_{u_z}\,i,x}\,(x,y)\,\psi_{z_{u_z}\,j,x}\,(x,y)\,\mathrm{d}x\,\mathrm{d}y\\
&+\int_{\mathcal{A}_z}\tilde{\sigma}_{yy}F_{\tau_{u_z}}\,(z)\,F_{s_{u_z}}\,(z)\,\mathrm{d}z\int_{\mathcal{A}_x}\int_{\mathcal{A}_y}\psi_{z_{u_z}\,i,y}\,(x,y)\,\psi_{z_{u_z}\,j,y}\,(x,y)\,\mathrm{d}x\,\mathrm{d}y\\
&+\int_{\mathcal{A}_z}\tilde{\tau}_{xy}F_{\tau_{u_z}}\,(z)\,F_{s_{u_z}}\,(z)\,\mathrm{d}z\int_{\mathcal{A}_x}\int_{\mathcal{A}_y}\psi_{z_{u_z}\,i,x}\,(x,y)\,\psi_{z_{u_z}\,j,y}\,(x,y)\,\mathrm{d}x\,\mathrm{d}y\Big]U_{z\tau_{u_z}j}\,(t)
\end{aligned}\tag{24}$$

The tracer δ_{wK} has been introduced in order to retain and/or discard the full nonlinear terms. In the latter case, namely $\delta_{wK}=0$, the von kármán approximation is assumed.

5.2.3. Virtual kinetic energy

Finally, the three non-zero contributions related to the δT, can be written as

$$\delta T^{u_x u_x} = \delta\dot{U}_{x\tau_{u_x} i}\,(t)\,\rho\Big[\int_{\mathcal{A}_z}F_{\tau_{u_x}}\,(z)\,F_{s_{u_x}}\,(z)\,\mathrm{d}z\int_{\mathcal{A}_x}\int_{\mathcal{A}_y}\psi_{x_{u_x}\,i}\,(x,y)\,\psi_{x_{u_x}\,j}\,(x,y)\,\mathrm{d}x\,\mathrm{d}y\Big]\dot{U}_{x\tau_{u_x}j}\,(t)$$

$$\delta T^{u_y u_y} = \delta\dot{U}_{y\tau_{u_y} i}\,(t)\,\rho\Big[\int_{\mathcal{A}_z}F_{\tau_{u_y}}\,(z)\,F_{s_{u_y}}\,(z)\,\mathrm{d}z\int_{\mathcal{A}_x}\int_{\mathcal{A}_y}\psi_{y_{u_y}\,i}\,(x,y)\,\psi_{y_{u_y}\,j}\,(x,y)\,\mathrm{d}x\,\mathrm{d}y\Big]\dot{U}_{y\tau_{u_y}j}\,(t)$$

$$\delta T^{u_z u_z} = \delta\dot{U}_{z\tau_{u_z} i}\,(t)\,\rho\Big[\int_{\mathcal{A}_z}F_{\tau_{u_z}}\,(z)\,F_{s_{u_z}}\,(z)\,\mathrm{d}z\int_{\mathcal{A}_x}\int_{\mathcal{A}_y}\psi_{z_{u_z}\,i}\,(x,y)\,\psi_{z_{u_z}\,j}\,(x,y)\,\mathrm{d}x\,\mathrm{d}y\Big]\dot{U}_{z\tau_{u_z}j}\,(t)\tag{25}$$

where being the density ρ a constant can be moved outside the integration operation.

5.3. Weak-form of the governing equations

By combining Eqs. (23), (24) and (25) with Eq. (18) and by assuming a simple harmonic motion $\{U_{\tau i}(t)\} = \left\{\hat{U}_{\tau i}\right\} e^{i\omega t}$, the weak-form of the GEs in their discretized form is obtained as follows

$$\delta\left\{\hat{U}_{\tau i}\right\}: \quad \left([K_{\tau s ij}] + \lambda_{ij}\left[K^{(\sigma)}_{\tau s ij}\right] - \omega^2_{ij}\,[M_{\tau s ij}]\right)\left\{\hat{U}_{s j}\right\} = \{0_{s j}\} \tag{26}$$

where $[K_{\tau s ij}]$, $\left[K^{(\sigma)}_{\tau s ij}\right]$ and $[M_{\tau s ij}]$ represent the stiffness, the initial stress and mass nuclei, respectively. Equation (26) can be alternatively written in a more explicitly form as

$$\delta\left\{\begin{array}{c}\hat{U}_{x_{\tau_{u_x} i}}\\ \hat{U}_{y_{\tau_{u_y} i}}\\ \hat{U}_{z_{\tau_{u_z} i}}\end{array}\right\}: \left(\left[\begin{array}{ccc} K_{\tau_{u_x} s_{u_x} ij} & K_{\tau_{u_x} s_{u_y} ij} & K_{\tau_{u_x} s_{u_z} ij}\\ K_{\tau_{u_y} s_{u_x} ij} & K_{\tau_{u_y} s_{u_y} ij} & K_{\tau_{u_y} s_{u_z} ij}\\ K_{\tau_{u_z} s_{u_x} ij} & K_{\tau_{u_z} s_{u_y} ij} & K_{\tau_{u_z} s_{u_z} ij}\end{array}\right] + \right.$$

$$\lambda_{ij}\left[\begin{array}{ccc} \delta_{vK}\, K^{(\sigma)}_{\tau_{u_x} s_{u_x} ij} & 0_{\tau_{u_x} s_{u_y} ij} & 0_{\tau_{u_x} s_{u_z} ij}\\ 0_{\tau_{u_y} s_{u_x} ij} & \delta_{vK}\, K^{(\sigma)}_{\tau_{u_y} s_{u_y} ij} & 0_{\tau_{u_y} s_{u_z} ij}\\ 0_{\tau_{u_z} s_{u_x} ij} & 0_{\tau_{u_z} s_{u_y} ij} & K^{(\sigma)}_{\tau_{u_z} s_{u_z} ij}\end{array}\right] -$$

$$\left.\omega^2_{ij}\left[\begin{array}{ccc} M_{\tau_{u_x} s_{u_x} ij} & 0_{\tau_{u_x} s_{u_y} ij} & 0_{\tau_{u_x} s_{u_z} ij}\\ 0_{\tau_{u_y} s_{u_x} ij} & M_{\tau_{u_y} s_{u_y} ij} & 0_{\tau_{u_y} s_{u_z} ij}\\ 0_{\tau_{u_z} s_{u_x} ij} & 0_{\tau_{u_z} s_{u_y} ij} & M_{\tau_{u_z} s_{u_z} ij}\end{array}\right]\right)\left\{\begin{array}{c}\hat{U}_{x_{s_{u_x} j}}\\ \hat{U}_{y_{s_{u_y} j}}\\ \hat{U}_{z_{s_{u_z} j}}\end{array}\right\} = \left\{\begin{array}{c} 0_{s_{u_x} j}\\ 0_{s_{u_y} j}\\ 0_{s_{u_z} j}\end{array}\right\} \tag{27}$$

Equation (27) allows us to carry out several thermoelastic vibration and stability analyses of the CNTRC plates under investigation by simply considering the solution of various eigenvalue problems.

6. Numerical results and discussion

The results have been computed by using highly stable trigonometric trial functions, for both simply-supported and clamped boundary condition, as shown in Eqs. (28) and (29). The classical acronym system [64, 65] has also been used to show the results. More specifically, the acronym $ED_{N_{ux}N_{uy}N_{uz}}$ has been employed, where E means that the classical equivalent single layer approach, for the plate kinematic description, has been introduced; D states that the Principle of Virtual Displacements (PVD) (or Hamilton's principle in the dynamic case) has been used in the analysis, and finally the three subscripts, N_{ux}, N_{uy} and N_{uz} are the expansion orders and represent independent free input parameters. Two different study

cases are proposed. The first one is related to the computation of the dimensionless eigenfrequency parameters $\hat{\omega} = \omega \frac{a^2}{h}\sqrt{\frac{\rho_m}{E_m}}$ of FG-CNT plates aimed to shown the high accuracy level obtained by the hierarchical modelling with respect to other methodologies present in literature.

Simply-supported plate

$$\begin{aligned}
\psi^{u_x}_{mn}(x,y) &= \sum_m^M \sum_n^N \cos\left(\frac{m\pi x}{a}\right) \sin\left(\frac{n\pi y}{b}\right);\\
\psi^{u_y}_{mn}(x,y) &= \sum_m^M \sum_n^N \sin\left(\frac{m\pi x}{a}\right) \cos\left(\frac{n\pi y}{b}\right);\\
\psi^{u_z}_{mn}(x,y) &= \sum_m^M \sum_n^N \sin\left(\frac{m\pi x}{a}\right) \sin\left(\frac{n\pi y}{b}\right);
\end{aligned} \tag{28}$$

Clamped plate

$$\begin{aligned}
\psi^{u_x}_{mn}(x,y) &= \sum_m^M \sum_n^N \sin\left(\frac{m\pi x}{a}\right) \sin\left(\frac{n\pi y}{b}\right);\\
\psi^{u_y}_{mn}(x,y) &= \sum_m^M \sum_n^N \sin\left(\frac{m\pi x}{a}\right) \sin\left(\frac{n\pi y}{b}\right);\\
\psi^{u_z}_{mn}(x,y) &= \sum_m^M \sum_n^N \sin\left(\frac{m\pi x}{a}\right) \sin\left(\frac{n\pi y}{b}\right);
\end{aligned} \tag{29}$$

The same investigation also shows the effect of the thermal environment on the modal characteristics of the FG-CNTRC plates made-up of temperature-dependent materials. The second study case deals with the buckling analysis of FG-CNTRC plates. Once again, the stability characteristics of the structure under investigation are analyzed and the respective dimensionless critical buckling loads $N^*_{cr} = N_{cr}\frac{b^2}{E_m h^3}$ due to axial and/or biaxial pre-stresses are compared and contrasted with those available in literature.

6.1. Free Vibration of FG-CNTRC Plates

A first validation of the proposed formulation is carried out for the case of free vibration analysis. For all of the numerical examples proposed in this section the material properties are those given by Eqs.(8) and (9) for the room temperature $T = 300\,K$. For the CNTs they can similarly be obtained from Table 1. For this specific case the considered volume fractions and related efficiency parameters are: $V^*_{CNT} = 0.11$ with $\eta_1 = 0.149$ and $\eta_2 = 0.934$;

$V^*_{CNT} = 0.14$ with $\eta_1 = 0.150$ and $\eta_2 = 0.941$; and $V^*_{CNT} = 0.17$ with $\eta_1 = 0.149$ and $\eta_2 = 1.381$. Beside, the assumptions $\eta_2 = \eta_3$ and $G_{12} = G_{13} = G_{23}$ are also made. Tables 3, 4 and 5 show the first six dimensionless frequency parameters of a simply-supported CNTRC square plate with CNT volume fraction $V^*_{CNT} = 0.11$, $V^*_{CNT} = 0.14$ and $V^*_{CNT} = 0.17$, respectively, and length-to-thickness ratio $a/h = 50$. In each of the aforementioned tables the CNTs are considered uniformly distributed (UD) and functionally graded according to three different laws: FG-V, FG-O and FG-X (see Eq.(1) for further details). By means of the hierarchical approach various theories have been tested and a good convergence is reached with the plate model ED_{555}. It should be borne in mind that the present hierarchical formulation has been derived in its generalized form, which means that the expansion orders of the displacement components are free parameters in the model. However, in this specific case, being the focus of the article on the investigation of the modal characteristics of the CNTRC plate, for convenience they have been increased simultaneously and uniformly. The results obtained by virtue of the HTRF have been compare with those computed by using the finite element (FE) commercial software Ansys [66], and with two formulations available in literature. The first one is a FSDT-based FEM and the second is a TSDT-based isogeometric formulation with non-uniform NURBS basis functions. In order to study the accuracy of the above mentioned methodologies both the average and the maximum difference, with respect to the FE software Ansys results, have been evaluated. From all of the proposed numerical examples the plate models ED_{444} and ED_{555} turned out to be the most accurate. The average $\Delta\%$ is significantly below the 0.5% in all of the addressed study cases, reaching its minimum of 0.12% in the specific case of $V^*_{CNT} = 0.14$ and CNTs distribution FG-X. It should also been highlighted the unsuitableness of the ED_{222} plate model which leads to higher average $\Delta\%$. However, the latter in the worst case scenario, related to $V^*_{CNT} = 0.17$ and CNTs distribution FG-O, is 4.23%. Before dealing with the fully clamped boundary condition a proper convergence analysis has been proposed in Table 6. The trigonometric trial functions given in Eq. (29) showed, as expected a high computational stability along with an acceptable rate of convergence. The convergence analysis has been carried out for the first six dimensionless frequencies of a CNTRC square plate and for all of the four CNTs distributions by using the ED_{555} plate model, $V^*_{CNT} = 0.11$ and a length-to-thickness ratio $a/h = 50$. Similarly to the simply-supported CNTRC plate case, Table 7, 8 and 9, show the first six dimensionless frequency of a fully clamped CNTRC square plate, with CNTs volume

fraction $V^*_{CNT} = 0.11$, $V^*_{CNT} = 0.14$ and $V^*_{CNT} = 0.17$, respectively. Once again the plate models ED_{444} and ED_{555} proved their high level of accuracy providing the best results. More specifically, the lowest average $\Delta\%$ is 0.98% obtained in the case of $V^*_{CNT} = 0.11$ and CNTs distribution UD, however with these models the average $\Delta\%$ never exceeded the 2% in all of the addressed study cases. The highest average $\Delta\%$ is 6.20% obtained by using ED_{222} plate model in the case of $V^*_{CNT} = 0.17$ and CNTs distribution FG-O.

6.2. Thermal effect on the modal characteristics of temperature-dependent FG-CNTRC Plates

The modal characteristics of temperature-dependent CNTRC plates are investigate in Figures 2 and 3. The temperature-dependency of both matrix and $(10, 10)$ single-walled carbon nanotube (SWCNT) (see Fig. 1 for more details) are given in Eqs. (8) and (9). Moreover, for comparison purpose, Table 1 shows the material properties of the SWCNT computed by using the molecular dynamics (MD) and for several temperature values ranging from $300\,K$ to $1000\,K$. Figure 2 depicts the effect of the thermal environment on the first three modes of a CNTRC square plate with volume fraction $V^*_{CNT} = 0.17$; efficiency parameters $\eta_1 = 0.142$, $\eta_2 = 1.626$ and $\eta_3 = 1.138$; length-to-thickness ratio $a/h = 40$ and UD, FG-O and FG-X CNTs distributions, respectively. Following this order, Fig. 2 (a), Fig. 2 (c) and Fig. 2 (e) refer to the simply-supported boundary condition (SSSS) whilst Fig. 2 (b), Fig. 2 (d) and Fig. 2 (f) to the fully clamped (CCCC) one. As expected, in either cases the modal characteristics are significantly affected by the temperature in both the pre- and post-buckled state. The modal interchange or mode shifting phenomenon occurs. In the CCCC case the mode veering between the second and the third mode is also observed. Being the critical temperature lower in the SSSS case than the CCCC case the temperature range of investigation has been chosen to be $300\,K - 500\,K$ and $300\,K - 700\,K$, respectively. Amongst the CNTs distributions analysed the FG-X showed the highest critical temperature and the FG-O the lowest one. In Fig. 3 the first, second and third mode of the three different CNTs distributions have been compared for both SSSS and CCCC boundary conditions.

6.3. Elastic Stability of FG-CNTRC Plates

A comprehensive elastic stability analysis, at room temperature $T = 300\,K$ for both axial and biaxial prestress conditions has been proposed in Tables 10 and 11, respectively. Various hierarchical plate models have been assessed. In both cases the critical buckling loads have been evaluated for simply-supported CNTRC square plate, with length-to-thickness ratio

$a/h = 100$, considering several values of the volume fraction $V^*_{CNT} = 0.11$, $V^*_{CNT} = 0.14$ and $V^*_{CNT} = 0.17$, with the same efficiency parameters used in the free vibration analysis, and for UD, FG-O and FG-X CNTs distributions. The results obtained with the proposed formulation have been compared with those available in literature and computed by using ISML-Ritz. The comparison showed an excellent agreement. For the same cases, the effect of the aspect ratio a/b has also been investigated in Fig. 4. The analysis showed that, for both axial and biaxial loadings the critical buckling load decreases when increasing the aspect ratio (a/b). Moreover, the highest critical buckling load is obtained by using a FG-X CNTs distribution and the lowest by using the FG-O one.

7. Conclusions

The present article investigated the thermoelastic vibration and the buckling characteristics of temperature-dependent carbon nanotube-reinforced composite (CNTRC) plates. The latter have been considered made up of four different types of uniaxially aligned reinforcements. More specifically, uniformly distributed (UD) and functionally graded (FG-V, FG-O and FG-X). The governing equations (GEs) have been derived by using Hamilton's principle (HP) in conjunction with higher order plate models hierarchically generated by using the method of power series expansion of displacement components. The GEs have been solved by using the Hierarchical Trigonometric Ritz Method (HTRM) based on highly stable trigonometric trial functions, leading to the Navier-type closed-form solution in the specific case of simply-supported boundary condition. From all of the carried out numerical investigations the following conclusions can be drawn:

- The use of higher order structural models is an absolute mandatory requirement when dealing with carbon nanotube-reinforced composites. In this respect, it has been observed that both for vibration and buckling analyses, the employment of the ED_{444} and ED_{555} plate models led to the highest level of results accuracy, when compared to commercial FEM software results, with respect to those proposed in literature and/or obtained by using the ED_{222}.

- In the specific case of free vibration of UD and FG CNTRC plates the ED_{444} and ED_{555} led to an average $\Delta\%$ of the first six dimensionless frequencies of less than the 0.5% in the case of simply-supported boundary condition and less than the 2% for the fully

clamped one. On the contrary, for the same two investigations the ED_{222} plate model led to an average $\Delta\%$ equal and higher than the 5%, respectively.

- The thermal environment affects dramatically the modal characteristics of the CNTRC plates. More specifically, modal interchange and/or modal shifting phenomena occurs repeatedly while increasing the temperature, in both the pre- and post-buckled state. Moreover, the FG-X CNTRC plate showed the highest critical temperature and the FG-O the lowest one.

- The elastic stability analysis showed that an increase of the simply-supported CNTRC plate aspect ratio leads to a significant reduction of the dimensionless critical buckling load. The CNTs distribution FG-X has the highest critical buckling load amongst those analysed whilst the FG-O the lowest.

References

[1] S. Iijima, Helical microtubules of graphitic carbon, Nature 354 (1991) 56–58.

[2] P. J. F. Harris, Carbon Nanotubes And Related Structures: New Materials for the 21st century, 1st Edition, Cambridge University Press, 1999.

[3] D. Qian, E. C. Dickey, R. Andrews, T. Rantell, Load transfer and deformation mechanisms in carbon nanotubes-polystyrene composites, Appl Phys Lett 76 (2000) 2868–2870.

[4] B. Fiedler, H. G. Florian, H. G. W. Malte, C. M. N. Mathias, S. Karl, Fundamental aspects of nano-reinforced composites, Composites Science and Technology 66 (16) (2006) 3115–3125.

[5] E. T. Thostenson, T. W. Chou, On the elastic properties of carbon nanotube-based composites: modeling and characterization, J Phys D 36 (2003) 573–582.

[6] M. F. Yu, O. Lourie, M. J. Dyer, K. Moloni, T. F. Kelly, R. S. Ruoff, Strength and breaking mechanism of multiwalled carbon nanotubes under tensile load, Science 287 (2000) 637–640.

[7] M. F. Yu, B. S. Files, S. Arepalli, R. S. Ruoff, Tensile loading of ropes of single wall carbon nanotubes and their mechanical properties, Phys Rev Lett 84 (2000) 5552–5555.

[8] C. Li, T. W. Chou, Elastic moduli of multi-walled carbon nanotubes and the effect of van der waals forces, Compos Sci Technol 63 (2003) 1517–1524.

[9] P. Zhu, Z. X. Lei, K. M. Liew, Static and free vibration analyses of carbon nanotube-reinforced composite plates using finite element method with first order shear deformation plate theory, Composite Structures 94 (4) (2012) 1450–1460.

[10] Z. X. Lei, K. M. Liew, J. L. Yu, Free vibration analysis of functionally graded carbon nanotube-reinforced composite plates using the element-free kp-ritz method in thermal environment, Composite Structures 106 (4) (2013) 128–138.

[11] P. Phung-Van, M. Abdel-Wahab, K. M. Liew, S. P. A. Bordas, H. Nguyen-Xuan, Isogeometric analysis of functionally graded carbon nanotube-reinforced composite plates using higher-order shear deformation theory, Composite Structures 123 (2015) 137–149.

[12] A. Alibeigloo, A. Emtehani, Static and free vibration analyses of carbon nanotube-reinforced composite plate using differential quadrature method, Meccanica 50 (1) (2015) 61–76.

[13] A. Alibeigloo, Three-dimensional thermoelasticity solution of functionally graded carbon nanotube reinforced composite plate embedded in piezoelectric sensor and actuator layers, Composite Structures 118 (1) (2014) 482–495.

[14] A. G. Arani, R. Rahmani, A. Arefmanesh, Elastic buckling analysis of single-walled carbon nanotube under combined loading by using the ansys software, Physica E: Low-dimensional Systems and Nanostructures 40 (7) (2008) 2390–2395.

[15] P. Malekzadeh, M. Shojaee, Buckling analysis of quadrilateral laminated plates with carbon nanotubes reinforced composite layers, Thin-Walled Structures 71 (2013) 108–118.

[16] M. C. Ray, R. C. Batra, Effective properties of carbon nanotube and piezoelectric fiber reinforced hybrid smart composites, Journal of Applied Mechanics 73 (3) (2009) 034503–034507.

[17] M. C. Ray, R. C. Batra, A single-walled carbon nanotube reinforced 13 piezoelectric composite for active control of smart structures, Smart Materials and Structures 16 (5) (2007) 1936–1947.

[18] L. W. Zhang, W. C. Cui, K. M. Liew, Vibration analysis of functionally graded carbon nanotube reinforced composite thick plates with elastically restrained edges, International Journal of Mechanical Sciences 103 (2015) 9–21.

[19] C. H. Thai, A. J. M. Ferreira, T. Rabczuk, H. Nguyen-Xuan, A naturally stabilized nodal integration meshfree formulation for carbon nanotube-reinforced composite plate analysis, Engineering Analysis with Boundary Elements (2017) In press, Corrected proofdoi:https://doi.org/10.1016/j.enganabound.2017.10.018.

[20] E. Garcia-Macias, L. Garcia-Macas, A. Saez, Bending and free vibration analysis of functionally graded graphene vs. carbon nanotube reinforced composite plates, Composite Structures 186 (2018) 123–138.

[21] M. Fallah, A. Daneshmehr, H. Zarei, H. Bisadi, M. G., Low velocity impact modeling of functionally graded carbon nanotube reinforced composite (FG-CNTRC) plates with arbitrary geometry and general boundary conditions, Composite Structures (2017) In press, corrected proofdoi:https://doi.org/10.1016/j.compstruct.2017.11.030.

[22] S. A. Fazelzadeh, S. Pouresmaeeli, G. E., Aeroelastic characteristics of functionally graded carbon nanotube-reinforced composite plates under a supersonic flow, Computer Methods in Applied Mechanics and Engineering 285 (2015) 714–729.

[23] R. Ansari, J. Torabi, A. H. Shakouri, Vibration analysis of functionally graded carbon nanotube-reinforced composite elliptical plates using a numerical strategy, Aerospace Science and Technology 60 (2017) 152–161.

[24] A. R. Setoodeh, M. Shojaee, Application of tw-dq method to nonlinear free vibration analysis of fg carbon nanotube-reinforced composite quadrilateral plates, Thin-WalledStructures 108 (2016) 1–11.

[25] P. Kumar, J. Srinivas, Vibration, buckling and bending behavior of functionally graded multiwalled carbon nanotube reinforced polymer composite plates using the layer-wise formulation, Composite Structures 177 (2017) 158–170.

[26] J. Jiang, L. Wang, Y. Zhang, Free Vibration of Isotropic, Orthotropic, and Multilayer Plates based on Higher Order Refined Theories, International Journal of Mechanical Sciences 122 (2017) 156–166.

[27] M. Wang, Z. M. Li, P. Quian, Semi-analytical solutions to buckling and free vibration analysis of carbon nanotube-reinforced composite thin plates, Composite Structures 144 (2016) 33–43.

[28] F. A. Fazzolari, A refined dynamic stiffness element for free vibration analysis of cross-ply laminated composite cylindrical and spherical shallow shells, Composites Part B: Engineering 62 (2014) 143–158.

[29] F. A. Fazzolari, M. Boscolo, J. R. Banerjee, An exact dynamic stiffness element using a higher order shear deformation theory for free vibration analysis of composite plate assemblies, Composite Structures 96 (2013) 262–278.

[30] F. A. Fazzolari, J. R. Banerjee, M. Boscolo, Buckling of composite plate assemblies using higher order shear deformation theoryan exact method of solution, Thin-Walled Structures 71 (2013) 18–34.

[31] F. A. Fazzolari, Advanced dynamic stiffness formulations for free vibration and buckling analysis of laminated composite plates and shells, Ph.D. thesis, City University London, uk.bl.ethos.635315 (7 2014).

[32] C. L. Zhang, H.-S. Shen, Temperature-dependent elastic properties od single-walled carbon nanotubes: Prediciton from molecular dynamics simulation, Applied Physical Letters 89 (2006) 081904–1–081904–4.

[33] C. L. Zhang, H.-S. Shen, Buckling and postbuckling of single-walled carbon nanotubes under combined axial compression and torsion in thermal environments, Phys. Rev. B 75 (2007) 045408–1–045408–7.

[34] H.-S. Shen, C. L. Zhang, Thermal buckling and postbuckling behavior of functionally graded carbon nanotube-reinforced composite plates, Materials & Design 31 (7) (2010) 3403–3411.

[35] H.-S. Shen, H. Wang, Nonlinear vibration of compressed and thermally postbuckled nanotube-reinforced composite plates resting on elastic foundations, Aerospace Science and Technology 64 (2017) 63–74.

[36] H. Wang, H.-S. Shen, Nonlinear vibration of nanotube-reinforced composite plates in thermal environments, Computational Materials Science 50 (8) (2011) 2319–2330.

[37] H.-S. Shen, H. Wang, D.-Q. Yang, Vibration of thermally postbuckled sandwich plates with nanotube-reinforced composite face sheets resting on elastic foundations, International Journal of Mechanical Sciences 124–125 (2017) 253–262.

[38] A. Alibeigloo, K. M. Liew, Thermoelastic analysis of functionally graded carbon nanotube-reinforced composite plate using theory of elasticity, Composite Structures 106 (1) (2013) 873–881.

[39] F. A. Fazzolari, Quasi-3D beam models for the computation of eigenfrequencies of functionally graded beams with arbitrary boundary conditions, Composite Structures 154 (2016) 239–255.

[40] F. A. Fazzolari, Generalized exponential, polynomial and trigonometric theories for vibration and stability analysis of porous fg sandwich beams resting on elastic foundations, Composites Part B: Engineering 136 (2018) 254–271.

[41] F. A. Fazzolari, Reissner's mixed variational theorem and variable kinematics in the modelling of laminated composite and FGM doubly-curved shells, Composites Part B: Engineering 89 (2016) 408–423.

[42] F. A. Fazzolari, Natural frequencies and critical temperatures of functionally graded sandwich plates subjected to uniform and non-uniform temperature distributions, Composite Structures 121 (2015) 197–210.

[43] F. A. Fazzolari, Fully coupled thermo-mechanical effect in free vibration analysis of anisotropic multilayered plates by combining hierarchical plates models and a trigonometric Ritz formulation., in: Mechanics of Nano, Micro and Macro Composite Structures Politecnico di Torino, 18-20 June, 2012.

[44] F. A. Fazzolari, Modal characteristics of P-and S-FGM plates with temperature-dependent materials in thermal environment, Journal of Thermal Stresses 39 (7) (2016) 854–873.

[45] F. A. Fazzolari, J. R. Banerjee, Axiomatic/asymptotic PVD/RMVT-based shell theories for free vibrations of anisotropic shells using an advanced Ritz formulation and accurate curvature descriptions, Composite Structures 108 (2014) 91–110.

[46] F. A. Fazzolari, Stability analysis of FGM sandwich plates by using variable-kinematics Ritz models, Mechanics of Advanced Materials and Structures 23 (4) (2016) 1104–1113.

[47] F. A. Fazzolari, Sandwich Structures, Elsevier, Woodhead Publishing, 2017, Ch. 2, pp. 49–90.

[48] J. D. Eshelby, The determination of the elastic field of an ellipsoidal inclusion, and related problems, Proc Roy Soc Lond, Ser A 241 (1957) 376–396.

[49] J. D. Eshelby, The elastic field outside an ellipsoidal inclusion, Proc Roy Soc Lond, Ser A 252 (1959) 561–569.

[50] T. Mori, K. Mori, Average stress in matrix and average elastic energy of materials with misfitting inclusions, Acta Metall 21 (1973) 571–574.

[51] L. W. Zhang, Z. X. Lei, K. M. Liew, An element free IMLS-Ritz framework for buckling analysis of FG-CNT reinforced composite resting on Winkler foundation, Engineering Analysis with Boundary Elements 58 (2015) 7–17.

[52] Y. Han, J. Elliott, Molecular dynamics simulations of the elastic properties of polymer/carbon nanotube composites, Computational Materials Science 39 (2007) 315–323.

[53] J. N. Reddy, Mechanics of laminated composite plates and shells. Theory and Analysis, 2nd Edition, CRC Press, 2004.

[54] R. M. Jones, Mechanics of composite materials, 2nd Edition, Taylor & Francis, United States, 1998.

[55] G. R. Kirchhoff, Über das Gleichgewicht und die Bewegung einer elastischen Sheibe. (About the equilibrium and motion of elastic bodies.), Journal für die Reine und Angewandte Mathematik 40 (1850) 51–88.

[56] E. Reissner, The effect of transverse shear deformation on the bending of elastic plates., Journal of Applied Mechanics 67 (1945) A67–A77.

[57] R. Mindlin, Influence of rotary inertia and shear on flexural motions of isotropic elastic plates., Journal of Applied Mechanics 18 (10) (1951) 31–38.

[58] K. Washizu, Variational Methods in Elasticity and Plasticity, 1st Edition, Pergamon, Headington Hill Hall, Oxford, 1968.

[59] H. Matsunaga, Free vibration and stability of functionally graded plates according to a 2-d higher-order deformation theory, Composite Structures 82 (4) (2008) 499–512.

[60] E. Carrera, A class of two-dimensional theories for anisotropic multilayered plates analysis, Atti Accademia delle scienze Torino, Memorie Scienze Fisiche 19-20 (1995) 49–87.

[61] E. Carrera, Theories and finite elements for multilayered plates and shells: a unified compact formulation with numerical assessment and benchmarking, Archives of Computational Methods in Engineering 10 (3) (2003) 216–296.

[62] W. Ritz, Über eine neue Methode zur Lösung gewisser Variationsprobleme der mathematischen Physik. (About a new method for the solution of certain variational problems of mathematical physics.), Journal für die Reine und Angewandte Mathematik 135 (1909) 1–61.

[63] J. N. Reddy, Energy Princiles and Variational Methods in Applied Mechanics, 2nd Edition, John Wiley & Sons, Inc., Hoboken, New Jersey, 2002.

[64] F. A. Fazzolari, E. Carrera, Accurate free vibration analysis of thermo-mechanically pre/post-buckled anisotropic multilayered plates based on a refined hierarchical trigonometric Ritz formulation., Composite Structures 95 (2013) 381–402.

[65] F. A. Fazzolari, E. Carrera, Coupled thermoelastic effect in free vibration analysis of anisotropic multilayered plates and fgm plates by using a variable-kinematics Ritz formulation, European Journal of Mechanics Solid/A, 44 (2014) 157–174.

[66] ANSYS v10.0 theory manual, ANSYS Inc., Southpointe, PA, 2006.

[67] C.-L. Zhang, H.-S. Shen, Temperature-dependent elastic properties of single-walled carbon nanotubes: Prediction from molecular dynamics simulations, Applied Physics Letters 89 (2006) 081904–1/081904–3.

Tables

Table 1: Temperature-dependent material properties for $(10, 10)$ SWCNT computed via MD [67].

Temperature	$E_{11}^{CNT}\,(TPa)$	$E_{22}^{CNT}\,(TPa)$	$G_{12}^{CNT}\,(TPa)$	$\alpha_{11}^{CNT}\,(10^{-6}/K)$	$\alpha_{22}^{CNT}\,(10^{-6}/K)$
300	5.6466	7.0800	1.9445	3.4583	5.1682
500	5.5308	6.9348	1.9643	4.5361	5.0189
700	5.4744	6.8641	1.9644	4.6677	4.8943
1000	5.2814	6.6220	1.9451	4.2800	4.7532

Table 2: Comparison of Young's modulii for PMMA/CNT reinforced composites at $T = 300\,K$

V_{CN}^{*}	MD[52]		ROM			
	$E_{11}\,(GPa)$	$E_{22}\,(GPa)$	$E_{11}\,(GPa)$	η_1	$E_{22}\,(GPa)$	η_2
0.12	94.6	2.9	94.78	0.137	2.9	1.022
0.17	138.9	4.9	138.68	0.142	4.9	1.626
0.28	224.2	5.5	224.50	0.141	5.5	1.585

Table 3: First 6 dimensionless frequency parameters of simply-supported UD and FG-CNTs reinforced composite plates with CNT volume fraction $V^*_{CNT} = 0.11$.

Theory	CNTs	Dimensionless circular frequency parameters							
		$\hat{\omega}_1$	$\hat{\omega}_2$	$\hat{\omega}_3$	$\hat{\omega}_4$	$\hat{\omega}_5$	$\hat{\omega}_6$	Ave. $\Delta\%$	Max $\Delta\%$
ANSYS[9]	UD	19.184	23.310	34.272	52.770	70.363	72.395		
FEM[9]		19.223	23.408	34.669	54.043	70.811	72.900	(0.90)	(2.37)
IGA[11]		19.093	22.968	34.017	53.664	70.808	72.569	(0.80)	(1.77)
ED_{555}		19.154724	23.273341	34.056917	51.964761	70.019200	72.128768	(0.41)	(1.43)
ED_{444}		19.154727	23.273346	34.056931	51.964806	70.019372	72.128951	(0.41)	(1.43)
ED_{333}		19.221850	23.337562	34.119735	52.045212	70.911035	73.021444	(0.80)	(1.27)
ED_{222}		19.352357	23.909889	35.580480	54.708048	71.124312	73.507819	(2.29)	(3.59)
ANSYS	FG-V	16.216	21.030	32.740	51.354	59.584	62.198		
FSDT		16.252	21.142	33.350	53.430	60.188	62.780	(1.43)	(4.04)
IGA		16.093	20.683	32.700	53.040	59.872	62.118	(1.07)	(3.28)
ED_{555}		16.179357	21.016365	32.753504	51.376757	59.185989	61.810534	(0.28)	(0.67)
ED_{444}		16.185794	21.021991	32.759051	51.383828	59.275523	61.895883	(0.22)	(0.51)
ED_{333}		16.229501	21.070030	32.821306	51.482582	59.865904	62.491816	(0.29)	(0.47)
ED_{222}		16.415851	21.786687	34.520642	54.490465	60.345530	63.317125	(3.24)	(6.11)
ANSYS	FG-O	14.290	19.274	31.013	49.326	52.569	55.362		
FSDT		14.302	19.373	31.615	51.370	53.035	55.823	(1.40)	(4.14)
IGA		14.153	19.154	31.711	52.422	52.616	55.123	(1.77)	(6.28)
ED_{555}		14.244495	19.273679	31.066976	49.422629	52.132323	54.961790	(0.37)	(0.83)
ED_{444}		14.246045	19.281061	31.085604	49.456969	52.135617	54.969339	(0.40)	(0.82)
ED_{333}		14.290482	19.320230	31.122404	49.505440	52.785186	55.607653	(0.30)	(0.44)
ED_{222}		14.502066	20.151149	33.048505	52.877584	53.158568	56.417744	(3.80)	(7.20)
ANSYS	FG-X	22.910	26.660	37.016	54.912	79.630	82.297		
FSDT		22.984	26.784	37.591	56.964	83.150	84.896	(2.28)	(4.42)
IGA		22.880	26.183	36.238	55.066	83.604	83.703	(1.83)	(4.99)
ED_{555}		22.899359	26.621053	36.939037	54.783982	79.413104	82.321825	(0.16)	(0.27)
ED_{444}		22.899576	26.622095	36.941792	54.788863	79.420116	82.321867	(0.15)	(0.26)
ED_{333}		23.012997	26.732435	37.048563	54.917445	79.617223	83.721663	(0.43)	(1.73)
ED_{222}		23.110938	27.190610	38.291257	57.253818	83.283214	83.871324	(2.85)	(4.59)

$\Delta\% = \frac{\|\omega^i_{FE} - \omega^i\|}{\|\omega^i\|} \times 100$

Table 4: First 6 dimensionless frequency parameters of simply-supported UD and FG-CNTs reinforced composite plates with CNT volume fraction $V^*_{CNT} = 0.14$.

Theory	CNTs	Dimensionless circular frequency parameters							
		$\hat{\omega}_1$	$\hat{\omega}_2$	$\hat{\omega}_3$	$\hat{\omega}_4$	$\hat{\omega}_5$	$\hat{\omega}_6$	Ave. $\Delta\%$	Max $\Delta\%$
ANSYS[9]	UD	21.311	25.192	35.866	54.320	77.629	79.482		
FEM[9]		21.354	25.295	36.267	55.608	78.110	80.015	(0.90)	(2.37)
IGA[11]		21.290	24.933	35.678	55.280	78.110	80.087	(0.80)	(1.77)
ED_{555}		21.316807	25.190847	35.685862	53.543395	77.389752	79.324843	(0.41)	(1.43)
ED_{444}		21.316811	25.190854	35.685877	53.543442	77.389970	79.325072	(0.41)	(1.43)
ED_{333}		21.407796	25.277658	35.767291	53.638524	78.558066	80.492722	(0.80)	(1.27)
ED_{222}		21.523244	25.802317	37.154424	56.212177	78.740381	80.918332	(2.29)	(3.59)
ANSYS	FG-V	17.956	22.531	34.052	52.739	65.893	68.315		
FSDT		17.995	22.643	34.660	54.833	66.552	68.940	(1.40)	(3.97)
IGA		17.879	22.222	34.013	54.412	66.438	68.506	(1.03)	(3.17)
ED_{555}		17.942047	22.539770	34.089285	52.791386	65.521810	67.951263	(0.24)	(0.56)
ED_{444}		17.950118	22.546752	34.095649	52.798782	65.630378	68.055287	(0.19)	(0.40)
ED_{333}		18.010588	22.611638	34.174749	52.916274	66.431454	68.861324	(0.50)	(0.82)
ED_{222}		18.181412	23.280738	35.805109	55.836993	66.897195	69.637341	(3.18)	(5.87)
ANSYS	FG-O	15.788	20.469	31.918	50.145	58.237	60.782		
FSDT		15.801	20.563	32.509	52.184	58.748	61.277	(1.36)	(4.07)
IGA		15.701	20.455	32.840	53.668	58.490	60.805	(1.83)	(7.03)
ED_{555}		15.762809	20.487997	31.992908	50.268185	57.840778	60.420071	(0.33)	(0.68)
ED_{444}		15.764676	20.496740	32.015213	50.309400	57.844896	60.429148	(0.36)	(0.67)
ED_{333}		15.821589	20.546817	32.059141	50.360497	58.660650	61.231256	(0.49)	(0.74)
ED_{222}		16.013895	21.333902	33.941566	53.696129	58.992078	61.962359	(3.72)	(7.08)
ANSYS	FG-X	25.474	29.065	39.257	57.272	82.437	90.389		
FSDT		25.555	29.192	39.833	59.333	87.814	91.299	(2.23)	(6.52)
IGA		25.528	28.616	38.313	56.981	85.793	92.220	(1.79)	(4.07)
ED_{555}		25.494920	29.049380	39.196075	57.155288	82.231606	90.413433	(0.13)	(0.25)
ED_{444}		25.495233	29.050924	39.200313	57.163023	82.242998	90.413497	(0.12)	(0.24)
ED_{333}		25.662265	29.212836	39.352315	57.332553	82.484937	92.380535	(0.64)	(2.20)
ED_{222}		25.746570	29.620180	40.494217	59.520313	85.946373	92.504353	(2.78)	(4.26)

$\Delta\% = \frac{\|\omega^i_{FE} - \omega^i\|}{\|\omega^i\|} \times 100$

Table 5: First 6 dimensionless frequency parameters of simply-supported UD and FG-CNTs reinforced composite plates with CNT volume fraction $V^*_{CNT} = 0.17$.

Theory	CNTs	Dimensionless circular frequency parameters							
		$\hat{\omega}_1$	$\hat{\omega}_2$	$\hat{\omega}_3$	$\hat{\omega}_4$	$\hat{\omega}_5$	$\hat{\omega}_6$	Ave. $\Delta\%$	Max $\Delta\%$
ANSYS[9]	UD	23.649	28.865	42.667	65.880	86.830	89.403		
FEM[9]		23.697	28.987	43.165	67.475	87.385	90.031	(0.93)	(2.42)
IGA[11]		23.528	28.440	42.362	67.018	87.328	89.569	(0.86)	(1.73)
ED_{555}		23.607166	28.813752	42.390850	64.861260	86.385312	89.054639	(0.58)	(1.55)
ED_{444}		23.607170	28.813759	42.390867	64.861313	86.385508	89.054849	(0.57)	(1.55)
ED_{333}		23.687237	28.890408	42.466526	64.960028	87.454626	90.125203	(0.61)	(1.40)
ED_{222}		23.840791	29.563775	44.179538	68.077089	87.705809	90.698715	(2.10)	(3.55)
ANSYS	FG-V	19.938	26.061	40.871	64.318	73.285	76.622		
FSDT		19.982	26.206	41.646	66.943	74.030	77.343	(1.45)	(4.08)
IGA		19.777	25.620	40.781	66.318	73.560	76.443	(1.07)	(3.11)
ED_{555}		19.898602	26.072204	40.952033	64.457195	72.839476	76.202418	(0.30)	(0.61)
ED_{444}		19.905218	26.079670	40.963255	64.475578	72.929427	76.288836	(0.27)	(0.49)
ED_{333}		19.962324	26.151511	41.071180	64.653916	73.673832	77.045250	(0.43)	(0.55)
ED_{222}		20.192625	27.048744	43.193616	68.405533	74.204475	78.014494	(3.36)	(6.36)
ANSYS	FG-O	17.529	23.659	38.109	60.652	64.581	68.011		
FSDT		17.544	23.783	38.855	63.179	65.154	68.579	(1.58)	(5.17)
IGA		17.398	23.754	39.579	64.620	65.571	67.836	(2.22)	(6.54)
ED_{555}		17.488469	23.713227	38.291799	60.968695	64.147499	67.652333	(0.44)	(0.67)
ED_{444}		17.485945	23.702780	38.263790	60.915618	64.127237	67.629872	(0.42)	(0.70)
ED_{333}		17.539211	23.777396	38.389754	61.127691	64.831470	68.335753	(0.49)	(0.78)
ED_{222}		17.815062	24.869534	40.925278	65.314737	65.570199	69.393428	(4.23)	(7.69)
ANSYS	FG-X	28.322	33.274	46.797	69.940	101.739	101.877		
FSDT		28.413	33.434	47.547	72.570	102.939	105.334	(1.79)	(3.76)
IGA		28.228	32.412	45.090	68.729	103.301	104.608	(2.09)	(3.65)
ED_{555}		28.267076	33.170785	46.636889	69.703620	101.370680	101.534726	(0.31)	(0.36)
ED_{444}		28.267778	33.173974	46.645177	69.718383	101.392357	101.535121	(0.30)	(0.34)
ED_{333}		28.430119	33.331665	46.799333	69.909919	101.694342	103.549252	(0.38)	(1.64)
ED_{222}		28.539922	33.844995	48.179079	72.488918	103.717839	105.730924	(2.47)	(3.78)

$\Delta\% = \frac{\|\omega^i_{FE} - \omega^i\|}{\|\omega^i\|} \times 100$

Table 6: Convergence analysis of the first 6 dimensionless frequency parameters of fully clamped UD and FG-CNTs reinforced composite plates with CNT volume fraction $V^*_{CNT} = 0.11$ and by using a ED_{555} plate model.

Frequency	CNTs	M, N					
	Distribution	4	6	8	10	12	14
$\hat{\omega}_1$	UD	42.812075	40.795355	40.164209	39.896015	39.760393	39.683430
$\hat{\omega}_2$		57.372793	46.904018	45.309396	44.645167	44.297950	44.092426
$\hat{\omega}_3$		101.978627	60.016601	57.259561	56.038208	55.367213	54.954512
$\hat{\omega}_4$		109.425118	99.144240	80.501128	76.777016	75.029009	74.025266
$\hat{\omega}_5$		160.856048	102.183022	98.185069	97.754274	97.527898	97.396026
$\hat{\omega}_6$		186.046331	102.578592	101.107178	100.464867	100.125601	99.852160
$\hat{\omega}_1$	FG-V	37.436613	35.244062	34.532846	34.222250	34.062039	33.969712
$\hat{\omega}_2$		53.660254	42.357020	40.571564	39.816899	39.418654	39.181397
$\hat{\omega}_3$		89.895326	56.826591	53.865035	52.542169	51.811638	51.360801
$\hat{\omega}_4$		98.448299	86.599576	78.511765	74.631952	72.803677	71.751666
$\hat{\omega}_5$		159.972540	90.741574	85.446473	84.917960	84.635760	84.468938
$\hat{\omega}_6$		180.194159	99.674840	88.996718	88.221496	87.806994	87.559700
$\hat{\omega}_1$	FG-O	33.728312	31.482112	30.735397	30.403804	30.231048	30.130901
$\hat{\omega}_2$		51.007183	38.987180	37.121225	36.326980	35.905654	35.653698
$\hat{\omega}_3$		81.687450	53.762488	50.738081	49.378344	48.624702	48.158520
$\hat{\omega}_4$		90.948176	78.032243	75.464790	71.537016	69.685253	68.618254
$\hat{\omega}_5$		159.051815	82.493365	76.747184	76.157040	75.841847	75.655587
$\hat{\omega}_6$		175.646660	91.869678	80.581181	79.728806	79.272460	79.000025
$\hat{\omega}_1$	FG-X	48.916891	47.123078	46.571290	46.338627	46.221221	46.154591
$\hat{\omega}_2$		62.208951	52.701982	51.253265	50.653206	50.340325	50.155412
$\hat{\omega}_3$		114.375562	65.178814	62.565838	61.415973	60.786079	60.399298
$\hat{\omega}_4$		121.086751	105.863625	85.299004	81.679288	79.982954	79.010720
$\hat{\omega}_5$		163.056135	111.842152	111.003488	108.466835	106.169478	104.831925
$\hat{\omega}_6$		188.527562	114.909741	113.303723	110.627434	110.429145	110.313177

Table 7: First 6 dimensionless frequency parameters of fully clamped UD and FG-CNTs reinforced composite plates with CNT volume fraction $V^*_{CNT} = 0.11$.

Theory	CNTs	Dimensionless circular frequency parameters							
		$\hat{\omega}_1$	$\hat{\omega}_2$	$\hat{\omega}_3$	$\hat{\omega}_4$	$\hat{\omega}_5$	$\hat{\omega}_6$	Ave. $\Delta\%$	Max $\Delta\%$
ANSYS[9]	UD	39.580	43.633	54.076	72.573	97.437	98.942		
FEM[9]		39.730	43.876	54.768	74.488	98.291	100.537	(1.22)	(2.64)
IGA[11]		40.332	44.438	55.894	78.249	101.566	103.738	(4.00)	(7.82)
ED_{555}		39.683430	44.092426	54.954512	74.025266	97.396026	99.852160	(0.98)	(2.00)
ED_{444}		39.683564	44.092570	54.954684	74.025519	97.397101	99.852635	(0.98)	(2.00)
ED_{333}		40.229315	44.607614	55.412097	74.440290	99.837674	100.286887	(2.12)	(2.57)
ED_{222}		40.399810	45.227050	56.972371	77.317605	100.062620	102.857380	(4.05)	(6.54)
ANSYS	FG-V	33.967	38.727	50.129	68.973	84.997	87.839		
FSDT		34.165	39.043	51.204	72.202	86.291	89.084	(1.86)	(4.68)
IGA		34.413	39.273	52.074	75.791	87.974	90.649	(3.86)	(9.89)
ED_{555}		33.969712	39.181397	51.360801	71.751666	84.468938	87.559700	(1.43)	(4.03)
ED_{444}		34.022715	39.228833	51.400790	71.786916	84.709464	87.790925	(1.41)	(4.08)
ED_{333}		34.390862	39.580215	51.730721	72.124871	86.489928	89.554257	(2.49)	(4.57)
ED_{222}		34.738907	40.483208	53.721439	75.574842	87.358698	90.784764	(4.95)	(9.57)
ANSYS	FG-O	30.161	35.165	46.811	65.631	76.338	79.376		
FSDT		30.303	35.444	47.878	68.842	77.468	80.460	(1.88)	(4.89)
IGA		30.452	35.843	49.533	74.080	78.417	81.422	(4.48)	(12.9)
ED_{555}		30.130901	35.653698	48.158520	68.618254	75.655587	79.000025	(1.71)	(4.55)
ED_{444}		30.134924	35.668922	48.195592	68.685486	75.663110	79.015704	(1.74)	(4.65)
ED_{333}		30.536643	36.029509	48.497001	68.950811	77.712747	81.015660	(2.71)	(5.06)
ED_{222}		30.841058	37.033215	50.797317	72.944260	78.159961	81.950943	(5.48)	(11.1)
ANSYS	FG-X	45.896	49.609	59.271	76.535	101.276	109.493		
FSDT		46.166	49.934	60.225	79.534	108.694	110.921	(2.57)	(7.32)
IGA		47.238	50.746	60.969	81.883	116.195	117.486	(6.18)	(14.7)
ED_{555}		46.154591	50.155412	60.399298	79.010720	104.831925	110.313177	(1.84)	(3.51)
ED_{444}		46.154788	50.156262	60.401601	79.015007	104.838136	110.313756	(1.85)	(3.52)
ED_{333}		47.000451	50.964426	61.130921	79.674642	105.512334	113.728674	(3.41)	(4.18)
ED_{222}		47.124097	51.448507	62.418705	82.135913	109.448834	113.877436	(5.18)	(8.07)

$\Delta\% = \frac{\|\omega^i_{FE} - \omega^i\|}{\|\omega^i\|} \times 100$

Table 8: First 6 dimensionless frequency parameters of fully clamped UD and FG-CNTs reinforced composite plates with CNT volume fraction $V^*_{CNT} = 0.14$.

Theory	CNTs	Dimensionless circular frequency parameters							
		$\hat{\omega}_1$	$\hat{\omega}_2$	$\hat{\omega}_3$	$\hat{\omega}_4$	$\hat{\omega}_5$	$\hat{\omega}_6$	Ave. $\Delta\%$	Max $\Delta\%$
ANSYS[9]	UD	43.426	47.237	57.288	75.445	101.841	105.539		
FEM[9]		43.583	47.479	57.968	77.395	106.371	106.487	(1.67)	(4.45)
IGA[11]		44.511	48.370	59.388	81.416	110.865	112.889	(5.38)	(8.86)
ED_{555}		43.595844	47.747259	58.214197	77.002138	102.818188	105.663813	(1.04)	(2.06)
ED_{444}		43.596003	47.747426	58.214392	77.002414	102.818688	105.665082	(1.04)	(2.06)
ED_{333}		44.305306	48.419530	58.810942	77.530358	103.343466	108.675392	(2.40)	(2.97)
ED_{222}		44.453519	48.979529	60.265969	80.274011	107.689319	108.861786	(4.42)	(6.40)
ANSYS	FG-V	37.357	41.857	52.906	71.567	92.669	95.324		
FSDT		37.568	42.175	53.963	74.785	94.022	96.573	(1.76)	(4.50)
IGA		38.013	42.588	54.963	78.458	96.503	98.985	(4.17)	(9.63)
ED_{555}		37.365457	42.300702	54.130008	74.368879	92.122273	95.010829	(1.37)	(3.92)
ED_{444}		37.429145	42.358178	54.178369	74.410358	92.396933	95.275823	(1.35)	(3.97)
ED_{333}		37.926161	42.832608	54.617283	74.841342	94.710871	97.566367	(2.70)	(4.58)
ED_{222}		38.260317	43.680245	56.510131	78.169231	95.571096	98.751888	(4.92)	(9.23)
ANSYS	FG-O	33.217	37.869	49.020	67.477	83.601	86.383		
FSDT		33.369	38.145	50.055	70.646	84.799	87.511	(1.79)	(4.70)
IGA		33.678	38.762	52.054	76.464	86.363	89.153	(4.96)	(13.3)
ED_{555}		33.198575	38.347877	50.357105	70.486192	82.938704	86.005844	(1.62)	(4.46)
ED_{444}		33.203179	38.365055	50.399502	70.563991	82.947643	86.023946	(1.66)	(4.57)
ED_{333}		33.703327	38.806196	50.740722	70.813562	85.433622	88.446634	(2.83)	(4.94)
ED_{222}		33.979997	39.755669	52.990808	74.802520	85.826068	89.294304	(5.38)	(10.9)
ANSYS	FG-X	50.125	53.706	63.184	80.410	105.403	117.701		
FSDT		50.403	54.025	64.112	83.394	112.896	119.134	(2.44)	(7.11)
IGA		51.893	55.194	65.003	85.524	121.074	125.823	(6.22)	(14.9)
ED_{555}		50.383571	54.238450	64.292261	82.875033	108.984563	118.441347	(1.73)	(3.40)
ED_{444}		50.383847	54.239724	64.295847	82.881918	108.994874	118.442051	(1.73)	(3.41)
ED_{333}		51.557753	55.363548	65.309273	83.782869	109.879754	122.898310	(3.69)	(4.42)
ED_{222}		51.662420	55.790586	66.477193	86.059415	113.565364	123.018073	(5.24)	(7.74)

$\Delta\% = \frac{\|\omega^i_{FE} - \omega^i\|}{\|\omega^i\|} \times 100$

Table 9: First 6 dimensionless frequency parameters of fully clamped UD and FG-CNTs reinforced composite plates with CNT volume fraction $V^*_{CNT} = 0.17$.

Theory	CNTs	Dimensionless circular frequency parameters							
		$\hat{\omega}_1$	$\hat{\omega}_2$	$\hat{\omega}_3$	$\hat{\omega}_4$	$\hat{\omega}_5$	$\hat{\omega}_6$	Ave. $\Delta\%$	Max $\Delta\%$
ANSYS[9]	UD	48.888	54.019	67.198	90.400	120.647	123.489		
FEM[9]		49.074	54.324	68.069	92.868	121.669	124.518	(1.11)	(2.73)
IGA[11]		49.777	54.982	69.447	97.561	125.557	128.316	(3.81)	(7.92)
ED_{555}		49.007391	54.585902	68.286948	92.262055	120.515946	123.715333	(0.88)	(2.06)
ED_{444}		49.007547	54.586069	68.287151	92.262357	120.517195	123.716614	(0.88)	(2.06)
ED_{333}		49.662550	55.203811	68.836165	92.763066	123.470561	125.190632	(2.09)	(2.61)
ED_{222}		49.863838	55.934481	70.671035	96.138377	123.737062	127.249257	(3.78)	(6.35)
ANSYS	FG-V	41.833	47.908	62.387	86.200	104.900	108.533		
FSDT		42.078	48.309	63.755	90.293	106.513	110.055	(1.88)	(4.75)
IGA		42.324	48.517	64.720	94.571	108.326	111.750	(1.54)	(4.35)
ED_{555}		41.882159	48.567382	64.095369	89.950501	104.394034	108.362304	(1.54)	(4.35)
ED_{444}		41.936580	48.620796	64.151460	90.016567	104.641680	108.603050	(1.55)	(4.43)
ED_{333}		42.402574	49.079745	64.613376	90.530614	106.896662	110.843864	(2.74)	(5.02)
ED_{222}		42.807571	50.218913	67.179378	94.996583	107.784370	112.213417	(5.20)	(10.2)
ANSYS	FG-O	37.073	43.228	57.568	80.745	94.059	97.793		
FSDT		37.247	43.577	58.890	84.717	95.462	99.142	(1.89)	(4.92)
IGA		37.443	44.308	61.620	92.497	96.479	100.327	(5.04)	(14.6)
ED_{555}		37.127393	43.998012	59.542239	84.860429	93.560166	97.719384	(1.84)	(5.10)
ED_{444}		37.141475	44.059893	59.686515	85.215517	93.580971	97.769905	(1.98)	(5.54)
ED_{333}		37.558833	44.431807	59.992774	85.478275	95.733005	99.865156	(3.01)	(5.86)
ED_{222}		37.982064	45.852798	63.257477	91.150351	96.345571	101.169734	(6.20)	(12.9)
ANSYS	FG-X	56.907	61.817	74.496	96.950	128.908	136.114		
FSDT		57.245	62.236	75.746	100.850	137.913	138.485	(2.62)	(6.99)
IGA		58.403	62.844	75.747	102.050	143.956	146.263	(5.06)	(11.7)
ED_{555}		57.004141	62.288487	75.723438	99.887283	133.203333	136.259960	(1.51)	(3.33)
ED_{444}		57.004761	62.291252	75.730851	99.901074	133.223827	136.260682	(1.52)	(3.35)
ED_{333}		58.222998	63.452273	76.776568	100.852807	134.215517	141.223329	(3.32)	(4.11)
ED_{222}		58.362429	63.996473	78.214532	103.578969	138.560548	141.392560	(4.88)	(7.49)

$\Delta\% = \frac{\|\omega^i_{FE} - \omega^i\|}{\|\omega^i\|} \times 100$

Table 10: Buckling of simply-supported UD and FG-CNTs reinforced composite plates axially loaded with $V^*_{CNT} = 0.11, 0.14, 0.17$, $a/b = 1$ and $b/h = 100$.

Theory	CNTs	Volume fraction			Ave. $\Delta\%$	Max $\Delta\%$
		0.11	0.14	0.17		
IMLS-Ritz [51]	UD	39.1158	49.0816	57.4776		
ED_{555}		39.334856	49.374527	60.443991	(2.11)	(5.16)
ED_{444}		39.334857	49.374528	60.443992	(2.11)	(5.16)
ED_{333}		39.406144	49.484275	60.549905	(2.30)	(5.35)
ED_{222}		39.946269	50.022968	61.342023	(3.59)	(6.72)
IMLS-Ritz	FG-O	21.3316	26.3572	31.2163		
ED_{555}		21.414541	26.484689	32.657457	(1.83)	(4.62)
ED_{444}		21.420788	26.493133	32.688792	(1.88)	(4.72)
ED_{333}		21.454885	26.542122	32.732285	(2.05)	(4.86)
ED_{222}		22.122609	27.223833	33.886651	(5.18)	(8.55)
IMLS-Ritz	FG-X	56.7373	71.5516	83.6142		
ED_{555}		57.106845	72.014264	88.091710	(2.22)	(5.36)
ED_{444}		57.108217	72.016497	88.096832	(2.22)	(5.36)
ED_{333}		57.256546	72.266440	88.361911	(2.53)	(5.68)
ED_{222}		57.747511	72.744511	89.048491	(3.32)	(6.50)

$$\Delta\% = \frac{\left\|N^*_{cr_o} - N^*_{cr_p}\right\|}{\left\|N^*_{cr_p}\right\|} \times 100$$

Table 11: Buckling of simply supported UD and FG-CNTs reinforced composite plates bi-axially loaded with $V^*_{CNT} = 0.11, 0.14, 0.17$, $a/b = 1$ and $b/h = 100$.

Theory	CNTs	Volume fraction			Ave. $\Delta\%$	Max $\Delta\%$
		0.11	0.14	0.17		
IMLS-Ritz [51]	UD	11.4103	13.2793	17.7656		
ED_{555}		11.549701	13.632032	17.911821	(1.57)	(2.66)
ED_{444}		11.549701	13.632033	17.911822	(1.57)	(2.66)
ED_{333}		11.566299	13.648468	17.936610	(1.70)	(2.78)
ED_{222}		12.139084	14.302295	18.780521	(6.60)	(7.70)
IMLS-Ritz	FG-O	7.7153	8.7948	12.0667		
ED_{555}		7.828845	8.928406	12.019023	(1.13)	(1.52)
ED_{444}		7.837719	8.939839	12.065473	(1.08)	(1.65)
ED_{333}		7.845862	8.951059	12.075687	(1.18)	(1.78)
ED_{222}		8.567793	9.687575	13.355731	(10.6)	(11.0)
IMLS-Ritz	FG-X	14.2345	16.2428	23.6906		
ED_{555}		14.593240	16.652545	23.548948	(1.88)	(2.52)
ED_{444}		14.595710	16.656560	23.558099	(1.88)	(2.55)
ED_{333}		14.618168	16.691424	23.599486	(1.95)	(2.76)
ED_{222}		15.613256	17.668386	24.891228	(7.84)	(9.69)

$$\Delta\% = \frac{\left\| N^*_{cr_o} - N^*_{cr_p} \right\|}{\left\| N^*_{cr_p} \right\|} \times 100$$

Figures

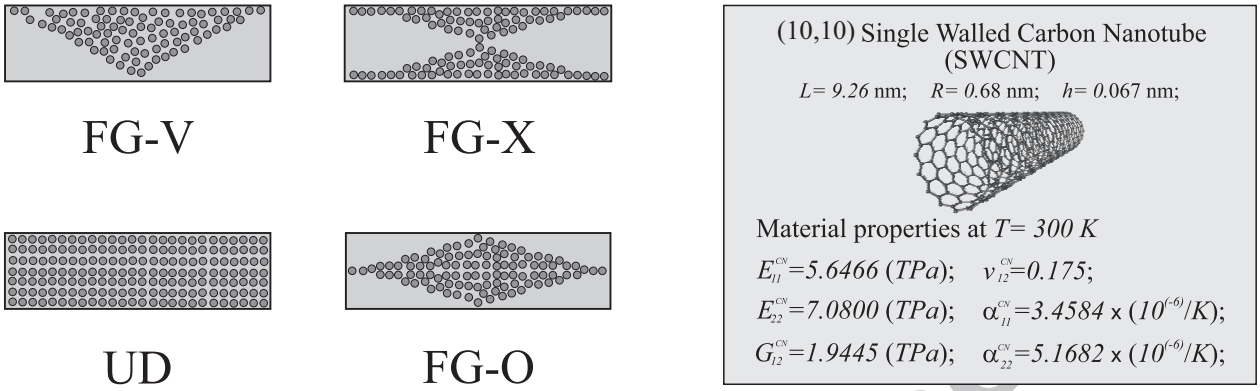

Figure 1: Carbon nanotube-reinforced plate configurations.

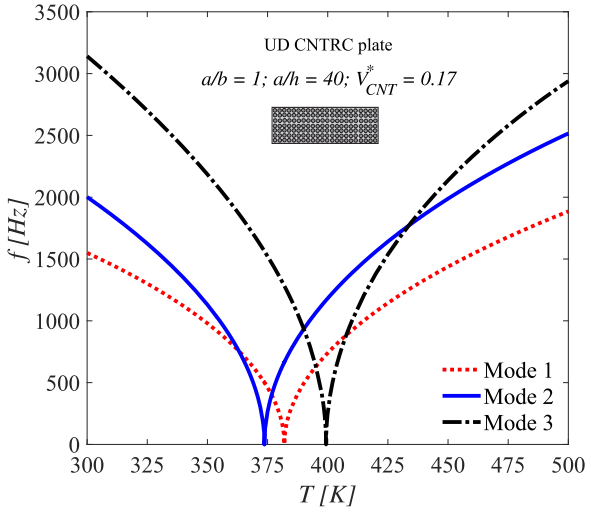

(a) Simply-supported plate

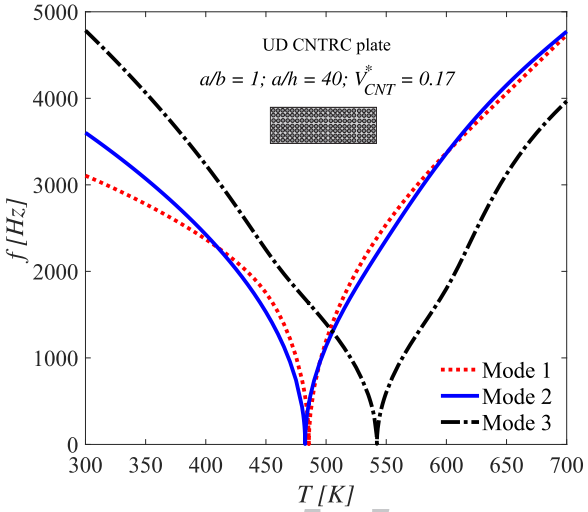

(b) Clamped plate

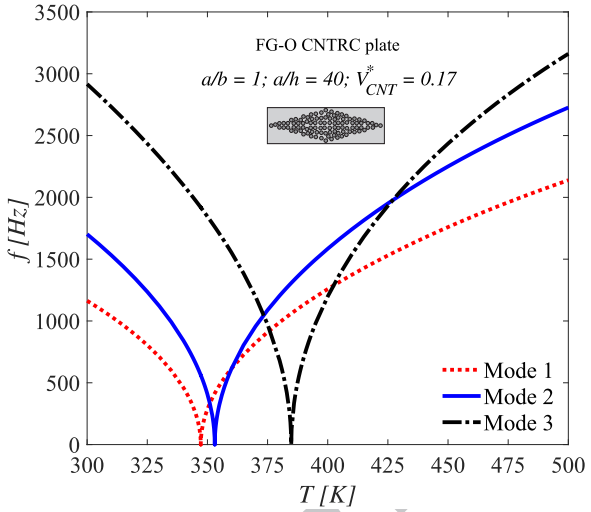

(c)

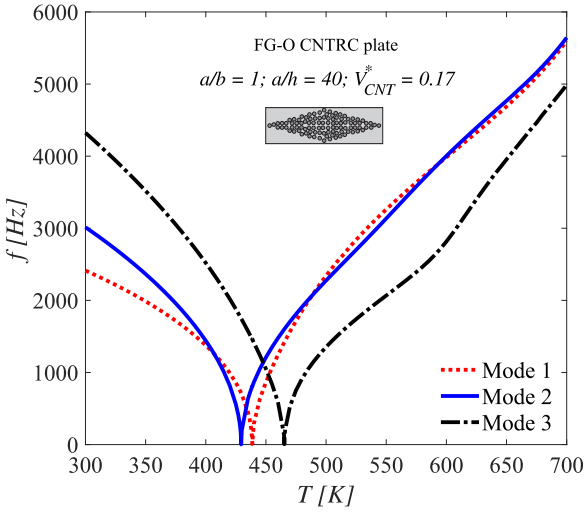

(d)

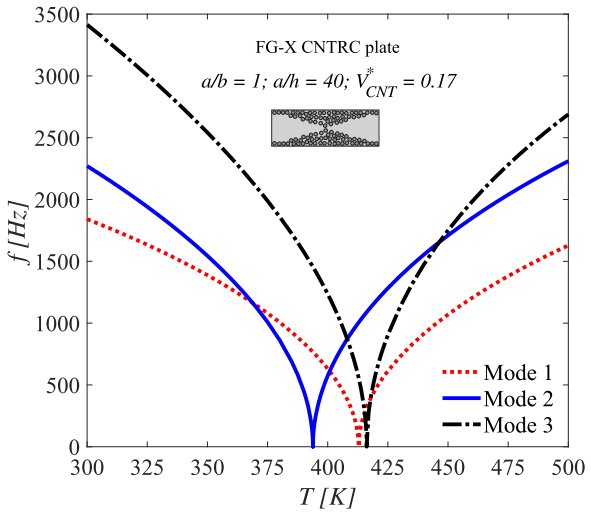

(e)

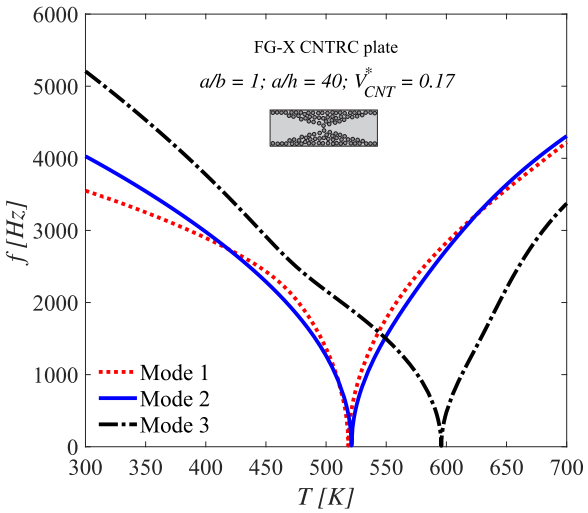

(f)

Figure 2: Effect of the thermal environment ont the first 3 modes of the temperature-dependent CNTRC plates: (a), (c) and (e) SSSS boundary condition; (b), (d) and (f) CCCC boundary condition;.

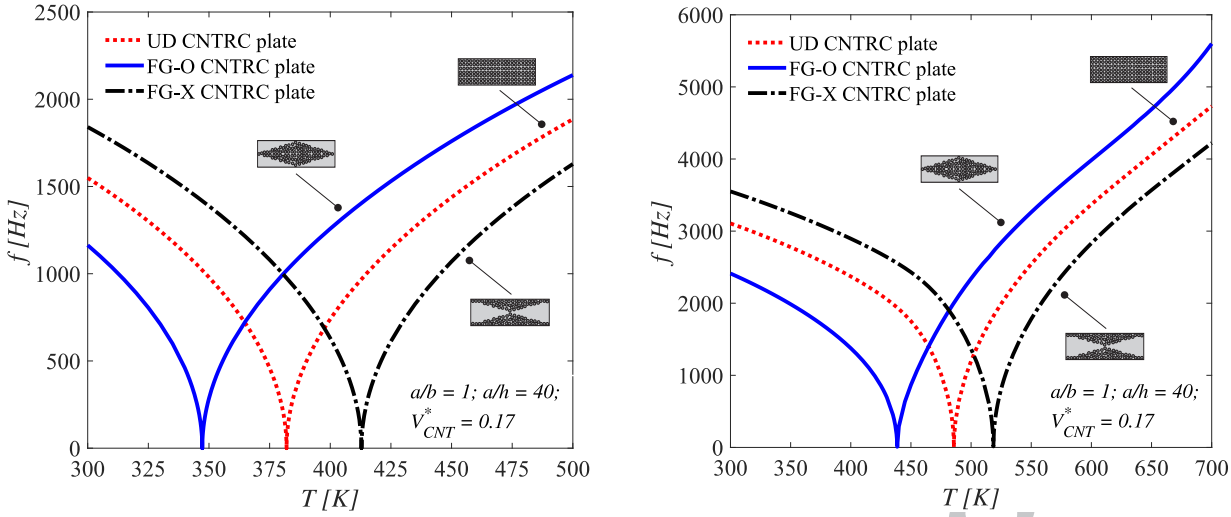

(a) Simply-supported plate

(b) Clamped plate

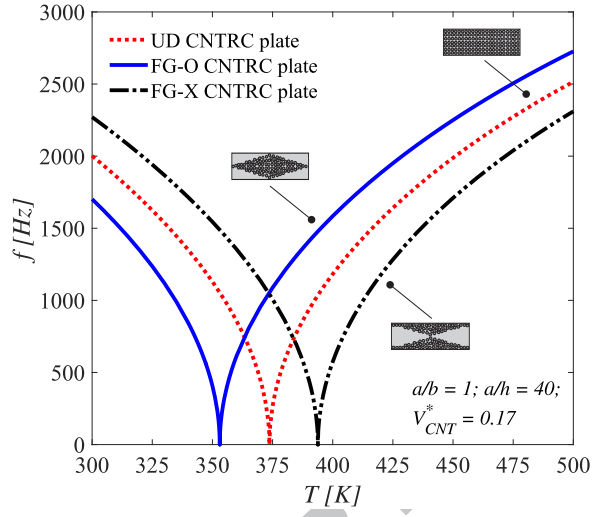

(c)

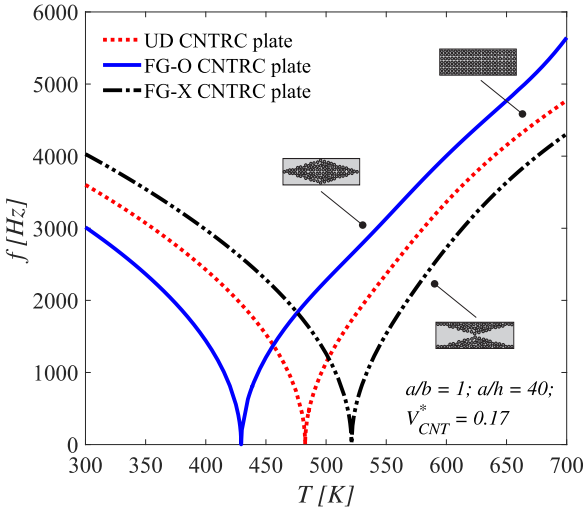

(d)

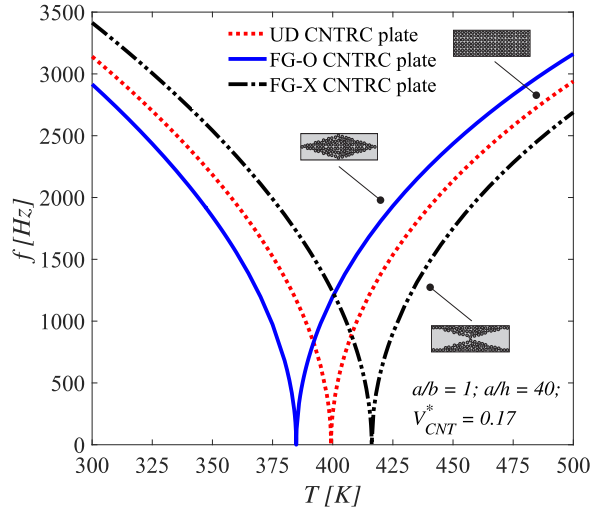

(e)

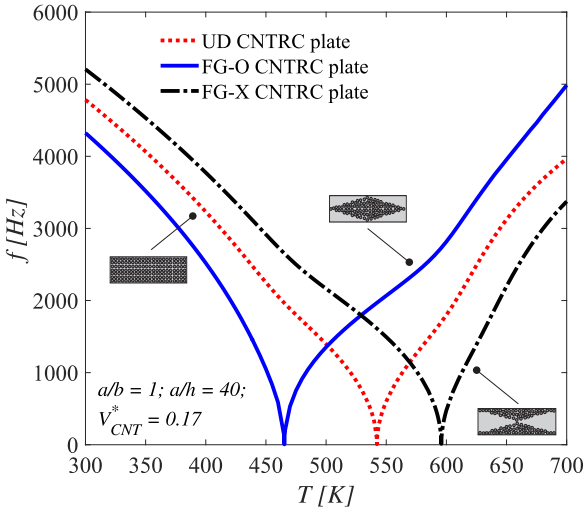

(f)

Figure 3: Effect of the thermal environment ont the first 3 modes of the temperature-dependent CNTRC plates: (a) and (b) - Mode 1; (c) and (d) - Mode 2; (e) and (f) - Mode 3.

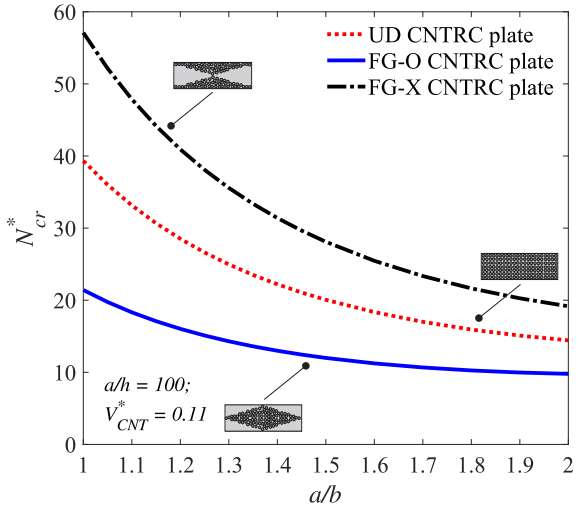

(a) $V^*_{CNT} = 0.11$

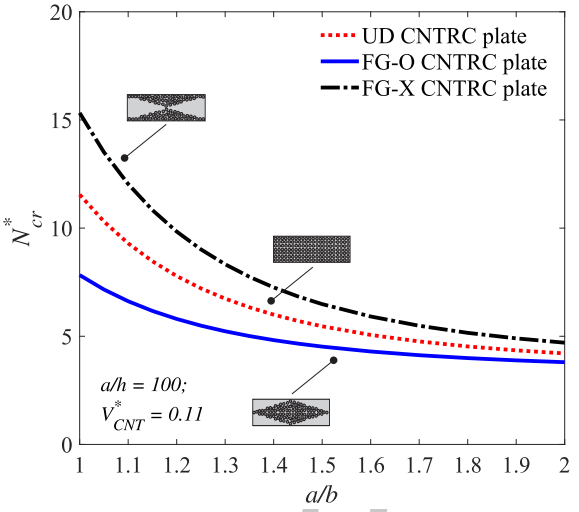

(b) $V^*_{CNT} = 0.11$

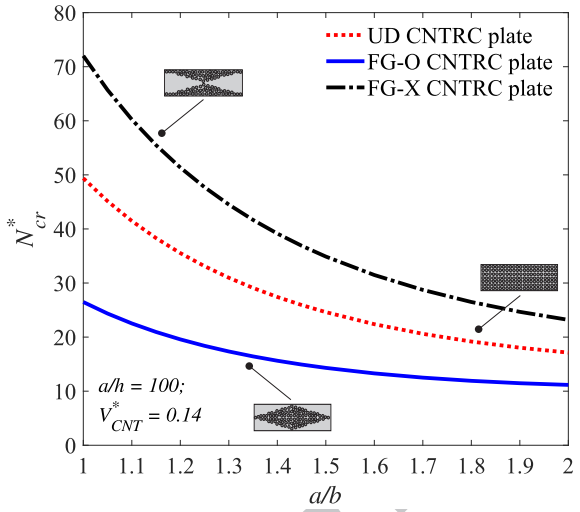

(c) $V^*_{CNT} = 0.14$

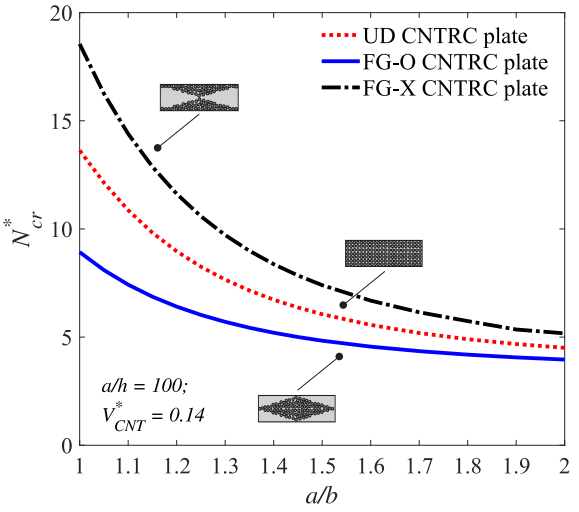

(d) $V^*_{CNT} = 0.14$

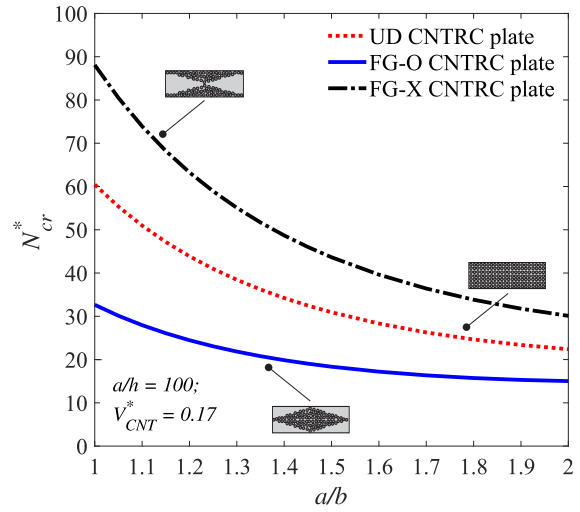

(e) $V^*_{CNT} = 0.17$

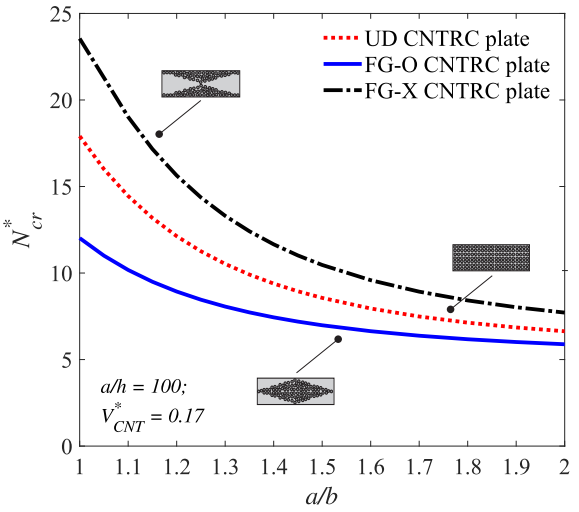

(f) $V^*_{CNT} = 0.17$

Figure 4: Dimensionless critical buckling load of CNTRC plates: (a), (c) and (e) - Axial buckling load; (b), (d) and (f) - Biaxial buckling load.